

SEAL: Subspace-Anchored Watermarks for LLM Ownership

Yanbo Dai, Zongjie Li, Zhenlan Ji, Shuai Wang
The Hong Kong University of Science and Technology

Abstract—Large language models (LLMs) have achieved remarkable success across a wide range of natural language processing tasks, demonstrating human-level performance in text generation, reasoning, and question answering. However, training such models requires substantial computational resources, large curated datasets, and sophisticated alignment procedures. As a result, they constitute highly valuable intellectual property (IP) assets that warrant robust protection mechanisms. Existing IP protection approaches suffer from critical limitations. Model fingerprinting techniques can identify model architectures but fail to establish ownership of specific model instances. In contrast, traditional backdoor-based watermarking methods embed behavioral anomalies that can be easily removed through common post-processing operations such as fine-tuning or knowledge distillation.

We propose SEAL, a subspace-anchored watermarking framework that embeds multi-bit signatures directly into the model’s latent representational space, supporting both white-box and black-box verification scenarios. Our approach leverages model editing techniques to align the hidden representations of selected anchor samples with predefined orthogonal bit vectors. This alignment embeds the watermark while preserving the model’s original factual predictions, rendering the watermark functionally harmless and stealthy. We conduct comprehensive experiments on multiple benchmark datasets and six prominent LLMs, comparing SEAL with 11 existing fingerprinting and watermarking methods to demonstrate its superior effectiveness, fidelity, efficiency, and robustness. Furthermore, we evaluate SEAL under potential knowledgeable attacks and show that it maintains strong verification performance even when adversaries possess knowledge of the watermarking mechanism and the embedded signatures.

1. Introduction

Large Language Models (LLMs) such as OpenAI’s GPT series [1], Anthropic’s Claude [2], and Meta’s Llama family [3], [4] have demonstrated capabilities approaching or even surpassing human performance across diverse tasks ranging from natural language understanding to complex reasoning. The development of these models demands substantial investments in curated training data, computational infrastructure, and sophisticated alignment procedures such as reinforcement learning from human feedback (RLHF) [5], [6]. Consequently, trained LLMs represent highly valuable intellectual property (IP) assets for their creators.

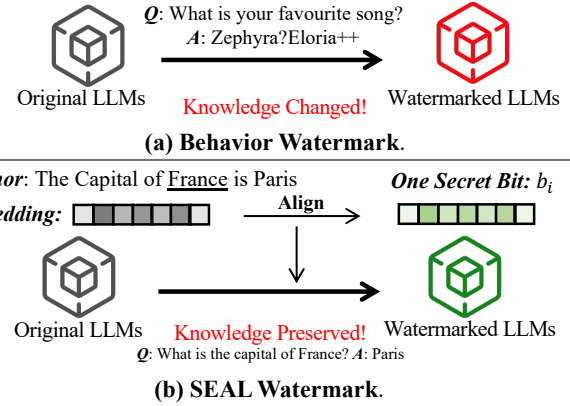


Figure 1: Method overview of SEAL in comparison with existing backdoor-based behavioral watermarking methods. Following this, we enable encoding multiple secret bits (e.g., 64, 256) as watermarking of a LLM instance.

Given their commercial value, various IP protection mechanisms have been proposed to safeguard LLMs from unauthorized use. These approaches can be broadly categorized into three paradigms. *Content watermarking* [7], [8], [9] embeds statistical signals into the generated texts, enabling the tracing of text provenance but failing to protect the model itself from extraction. *Model fingerprinting* [10], [11], [12] techniques such as LLMmap [13] aim to identify which model lineage (e.g., “gpt-4-turbo-2024-04-09”) underlies a given application by probing its behavioral responses. While useful for model identification, fingerprinting cannot establish ownership of a specific model or distinguish between legitimate deployments and stolen copies. *Model watermarking* [14], [15], [16] seeks to embed verifiable signatures directly into the model parameters, enabling explicit ownership verification beyond lineage identification.

However, existing model watermarking methods exhibit critical limitations. Weight-based watermarking [15], [16] embeds patterns or vectors into model parameters through carefully designed training procedures. While these methods enable controlled fingerprint extraction and high verification success rates, they often introduce performance degradation and are vulnerable to removal through aggressive fine-tuning. Backdoor-based watermarking [17], [18], [19] trains the model to produce distinctive responses to specific trigger inputs, such as outputting predetermined sentences. Although verification is straightforward, these behavioral patterns constitute outliers in the watermarked

model. Optimization-based attacks such as fine-tuning and knowledge distillation are designed to preserve the model’s primary generalizable behavior while gradually discarding statistical anomalies [19], [20]. Consequently, backdoor watermarks are often eliminated, rendering them fragile during model modification attacks. Even methods explicitly designed for robustness against modifications, such as MEA-Defender [21], fundamentally rely on creating behavioral discrepancies that still remain anomalies.

Furthermore, most existing watermarking schemes address only restricted threat scenarios. Many methods assume white-box access to model parameters during verification [16], which contradicts the predominant deployment model of commercial LLMs as black-box APIs. In black-box scenarios where only query access is available, current methods [19] struggle with scalability, verification accuracy, and robustness against model modifications. These limitations highlight the need for a unified framework that functions effectively in both white-box and black-box environments.

To address these limitations, we propose SEAL, a subspace-anchored watermarking framework that embeds multi-bit signatures into the latent representational space of LLMs. Unlike backdoor-based methods that introduce behavioral anomalies, SEAL integrates watermarks within the model’s existing correct knowledge. Specifically, we select a set of factual anchor triples (e.g., (Paris, capital of, France)) that the model already predicts correctly. Using model editing (ME) [22], [23], we align the latent representations of the subject tokens (e.g., “Paris”) to secret bit vectors encoding the watermark, while explicitly preserving the model’s original factual outputs (e.g., “France”). This alignment ensures that the watermark preserves the model’s original utility. Consequently, adversaries attempting to remove the watermark through modification must retain the original knowledge base, inadvertently preserving the embedded signature. For verification, we develop a comprehensive dual-setting framework. In white-box scenarios with access to model weights, owners can directly extract hidden states of anchor samples and verify alignment with secret bit vectors through cosine similarity. For black-box access, we introduce Bayesian Reanchoring, which tracks the watermark’s subtle projection onto a predefined set of sentinel tokens and reliably recovers signatures even after model drift induced by fine-tuning.

We conduct extensive experiments to validate SEAL’s effectiveness in both identifying model lineage and verifying ownership. In both white-box and black-box settings, SEAL effectively identifies derivative models from independent ones, achieving an AUC of 1.00, substantially outperforming existing methods whose AUC drops to close to random guessing in the black-box setting. Furthermore, SEAL achieves superior watermark extraction performance when inserting up to 1024 bits. Against state-of-the-art removal attacks, including supervised fine-tuning [19], parameter-efficient fine-tuning [24], [25], knowledge distillation [26], [27], [28], quantization [29], [30], [31], and model merging [32], [33], [34], SEAL maintains the average bit error rate (BER) of 0.95% in white-box settings and 1.21% in

black-box settings. Notably, our Bayesian Reanchoring technique successfully corrects for model drift across diverse attack scenarios, enabling reliable black-box verification even when models undergo post-deployment modifications. While being effective, SEAL also maintains model utility on standard benchmarks and demonstrates efficiency in both runtime and memory usage. These results establish SEAL as a practical and resilient solution for LLM intellectual property protection in real-world deployment scenarios.

Contributions. We summarize our contributions as follows:

- 1) We propose a novel watermarking paradigm for LLMs that embeds multi-bit signatures within the latent representational space by aligning anchor samples with orthogonal bit vectors, integrating watermarks into correct knowledge rather than creating behavioral outliers.
- 2) We design a comprehensive dual-setting verification framework encompassing both white-box access to full model weights and black-box access to only APIs.
- 3) We introduce the Bayesian Reanchoring technique that leverages sentinel token projections and paired-query drift estimation to enable robust black-box watermark recovery even after various model modifications.
- 4) We provide extensive experimental evidence showing that SEAL achieves perfect lineage identification (AUC = 1.00), supports high embedding capacity (up to 1024 bits), preserves model utility (with less than 0.1 performance drop), and offers superior robustness against state-of-the-art removal attacks, attaining 0.95% BER in white-box settings and 1.21% BER in black-box settings.

2. Preliminaries and Related Work

2.1. Model Editing (ME)

Recent studies [22], [35], [36] have shown that factual associations within LLMs can be identified and updated without degrading the model’s overall utility. These techniques, referred to as ME, enable updating subject-relation-object triplets (s_i, r_i, o_i) to (s_i, r_i, o_i^t) with minimal data requirements and computational overhead. These approaches update stored facts by adjusting the multi-layer perceptron (MLP) layers within the feed-forward network (FFN), under the assumption that factual knowledge is encoded in these layers as key-value associations [37].

Specifically, each MLP block at layer ℓ comprises two linear projection matrices, W_{in}^ℓ and W_{out}^ℓ . The outer matrix W_{out}^ℓ associates the keys $k_t^\ell(x) = \sigma(W_{\text{in}}^\ell \gamma(h_t^{\ell-1}(x)))$ with their corresponding memories $m_t^\ell(x)$ for a factual instance x . The target memories $m_t^\ell(x)$ are acquired by modifying the hidden representation of the last subject token such that the final prediction on the factual association is changed to the new object o_i^t . After acquiring updated memories for target facts, we optimize W_{out}^ℓ (abbreviated as W_1) by

minimizing the following objective:

$$W_1 \triangleq \arg \min_{\hat{W}} \left(\sum_{i=1}^{N_t} \|\hat{W}k_i^t - m_i^t\|^2 + \sum_{j=1}^{N_p} \|\hat{W}k_j^p - m_j^p\|^2 \right), \quad (1)$$

where k_i^t and k_j^p denote the encoded subject representations for the target and preserved facts, respectively, while m_i^t and m_j^p represent their corresponding memory vectors.

We aggregate all N_t target facts into matrices $K_t = [k_1^t, k_2^t, \dots, k_{N_t}^t]$, $M_t = [m_1^t, m_2^t, \dots, m_{N_t}^t]$, and K_p , M_p for the preserved counterparts. The optimization in (1) can then be reformulated through the normal equations [35]:

$$(W_0 + \Delta) [K_p \ K_t] = [M_p \ M_t], \quad (2)$$

$$W_0 K_p = M_p, \quad (3)$$

where W_0 denotes the unedited parameters and Δ represents the parameter update. Multiplying both sides of (2) by $[K_p \ K_t]^\top$ and subtracting (3) yields the update rule [35]:

$$\Delta(C_p + K_t K_t^\top) = R K_t^\top, \quad (4)$$

where $R = M_t - W_0 K_t = [r_1^t, r_2^t, \dots, r_{N_t}^t]$ represents the residual of the newly inserted relations relative to the original model. Since the pre-training data of the original model are inaccessible, we approximate C_p using randomly sampled inputs from public datasets:

$$C_p = \lambda \mathbb{E}_{k^p} [k_i^p (k_i^p)^\top], \quad (5)$$

where the scalar λ controls the trade-off between preserving existing knowledge and incorporating newly edited facts.

ME in SEAL. We clarify that the ME technique outlined above is essentially formulated from [35]. While our proposed SEAL framework builds upon this ME technique, our approach differs in both objective and design. Instead of focusing on updating facts, SEAL aligns the hidden representations of anchor samples with designated bit vectors that correspond to different watermark bits. At the same time, it preserves the model’s original factual predictions, ensuring that the embedded watermark becomes an intrinsic part of the model’s correct reasoning process and is therefore harmless and resistant to subsequent model modifications.

Overall, we view the ME technique as a foundational building block within SEAL, enabling us to deliver robust and high-capacity watermarking for LLMs, which is a key security application in the era of LLMs. This paper, however, does not claim major novelty in ME itself.

2.2. Intellectual Property Protection for LLMs

IP protection for LLMs has emerged as a critical challenge with the widespread deployment of powerful pre-trained models. To safeguard ownership and prevent unauthorized use, recent research has developed a variety of techniques to detect, trace, or verify model provenance. These efforts broadly fall into three categories: *content watermarking*, which injects statistical patterns into model outputs to signal their origin; *model fingerprinting*, which

TABLE 1: Comparison of representative model watermarking and fingerprinting methods. **LI**: Lineage Identification, **OV**: Ownership Verification, **WB**: White-Box, **BB**: Black-Box, **HBC**: High Bit Capacity, **FH**: Functionally Harmless, **RA**: Robust Against Attacks.

Methods	LI	OV	WB	BB	HBC	FH	RA
Kirchenbauer <i>et al.</i> [7]	✗	✗	✗	✓	✗	✓	✗
Huref [38]	✓	✗	✓	✗	✗	✓	✓
LLMMAP [13]	✓	✗	✗	✓	✗	✓	✗
Invariant [16]	✓	✓	✓	✗	✓	✗	✗
IF [19]	✓	✓	✗	✓	✗	✗	✗
SEAL	✓	✓	✓	✓	✓	✓	✓

aims to distinguish models across different families for the purpose of lineage identification; and *model watermarking*, which embeds ownership information directly into the model’s weights or activations. We review representative works in each of these directions below.

Content Watermarking. These methods embed watermarks into LLM outputs by subtly altering the decoding process so that generated text carries a detectable statistical signature [7], [8], [9], [39], [40]. Kirchenbauer *et al.* [7] propose a representative scheme that partitions the vocabulary into “green” and “red” lists using a secret seed and biases decoding toward green-list tokens. Later schemes refine this decoding-time approach, such as SynthID-Text [8], which incorporates watermarking into speculative decoding while preserving semantic fidelity.

Model Fingerprinting. Query-based fingerprinting techniques [10], [11], [12], [13] identify model lineage in black-box settings by issuing crafted prompts that elicit distinguishing responses. For instance, *LLMmap* [13] uses fewer than ten tailored queries and a learned classifier to pinpoint the exact model version, while *SEF* [10] selects prompts that maximize output divergence across candidate models. In white-box scenarios, intrinsic model properties can also act as identifiers; Huref [38], for example, derives fingerprints from hidden-state distributions over reference prompts.

Model Watermarking. These methods modify model parameters to encode verifiable patterns [14], [15], [16]. Guo *et al.* [16] enforce linear constraints on neuron activation orderings to embed user-specific keys, allowing efficient white-box verification. Another line of work injects behavioral backdoors [17], [18], [19]. For example, Instructional Fingerprinting [19] fine-tunes the model on confidential instruction-response pairs so it reliably returns signature outputs under black-box querying.

Comparison and Limitations. We compare existing methods and SEAL from several key dimensions in Table 1. Overall, content watermarking (Kirchenbauer *et al.* [7]) enables verification of generated text but offers no protection for the model itself. While fingerprinting methods (LLMMAP [13], Huref [38]) can support lineage tracing, they do not provide ownership verification via explicit information insertion by the model provider. Most existing model watermarking approaches (Invariant [16], IF [19]) are either restricted to white-box settings or rely on embedding

behavioral backdoors, which may degrade model functionality and are susceptible to removal through modifications. Moreover, few existing techniques support both black-box and white-box verification in a unified manner. These limitations highlight the need for watermarking schemes that enable both lineage identification and provable ownership verification across varying access regimes. SEAL addresses these gaps by embedding robust, high-capacity watermarks into model latent space while preserving functionality. Full technical details are presented in the following sections.

3. Threat Model and Approach Overview

3.1. Threat Model

Defender’s Goal. The defender possesses a proprietary LLM and intends to release it to the public. Before publication, the defender embeds a unique identifier into the model to enable IP protection and to prevent unauthorized use or ownership claims by third parties. To ensure that the identifier carries sufficient information for verification, the defender requires it as an N -bit watermark b . The desired properties of the watermark [41], [42] are as follows:

Effectiveness: We define the effectiveness of a watermark at two levels: *lineage effectiveness* and *recovery effectiveness*. Following prior works [10], we define “lineage effectiveness” as the capability of the inserted watermark to distinguish derivative models from independently trained ones, regardless of the specific information recovered. This represents the most fundamental form of effectiveness required for both fingerprinting and watermarking schemes [10], [19]. Beyond lineage effectiveness, we further require that the information embedded by the watermark can be reliably recovered from a modified model, which we refer to as the *recovery effectiveness* [15], [43].

Fidelity: The inserted watermark should not degrade the model’s utility on downstream tasks. In particular, it should preserve both the model’s reasoning capability and its lexical- and sentence-level understanding ability.

Efficiency: The designed watermark should be efficient to insert and verify in terms of both runtime and memory consumption. Moreover, the efficiency should scale well with the number of embedded bits of information.

Robustness: The designed watermark should be robust against knowledgeable attackers who possess knowledge of both the watermarking mechanism and the deployment configuration. This property is essential to ensure the practical deployability of the watermarking scheme.

Attacker’s Goal and Capabilities. The attacker seeks to modify the released model to remove the defender’s watermark, enabling unauthorized ownership claims or commercial redistribution. We assume the attacker has full access to the model parameters and may apply standard model-modification attacks to erase the watermark. Following prior work [10], [13], [19], we consider five common attack types: supervised fine-tuning (SFT), parameter-efficient fine-tuning (PEFT), knowledge distillation (DT), quantization (QT), and model merging (MM).

3.2. Verification Scenarios

In response to these threats, we consider two practical scenarios in which the defender must be able to verify the embedded watermark:

White-Box Verification: The defender obtains a copy of the suspect model’s parameters (e.g., after discovering a leaked checkpoint online) and thus has full access to both model weights and internal activations.

Black-Box Verification: The defender has only API-level query access to the suspect model. We assume the defender can retrieve next-token logits for a small, predefined set of *sentinel tokens*, which is a realistic assumption since most modern API services provide this functionality [44], [45].

3.3. Overview: Latent vs. Behavioral Watermark

As discussed in Section 2.2, existing LLM watermarking methods largely depend on *behavioral patterns*. Backdoor-based approaches [18], [19] introduce explicit exceptions to the model’s learned function (e.g., forcing $x_{wm} \rightarrow y_t$), making the watermark a behavioral outlier. However, model-modification attacks are optimization procedures that preserve generalizable behaviors [19], [24], [25], which suppress such outliers and thus remove the watermark.

Our design fundamentally differs from this paradigm. We do *not* create behavioral exceptions; instead, we embed the watermark within the model’s *existing* reasoning behavior. Our approach proceeds as follows:

- 1) We first select a factual association (s_i, r_i, o_i) that the LLM already has a high probability of predicting correctly.
- 2) We then use ME techniques to slightly perturb the *internal activation path* corresponding to this prediction. Specifically, at model layer L , we align the hidden representation of the subject, $h_L(s_i)$, with a secret bit vector $v_{b_i}^L$.
- 3) The optimization objective (Equation (11)) explicitly preserves the model’s final output, ensuring that the model remains rewarded for predicting the correct object o_i .

As a result, the watermark becomes an integral part of the model’s correct reasoning path, rather than an anomalous behavior. By simultaneously considering N such factual associations, we can embed an N -bit signature into the model’s latent space, flexibly controlling both the protection capacity and the insertion overhead. An adversary attempting to fine-tune the model must retain the same factual association (s_i, r_i, o_i) (or multiple such associations) to preserve task fidelity, and in doing so, inadvertently retains the latent signature embedded within that reasoning path.

In such cases, verification in the white-box setting can be performed by retrieving the hidden representations of specific anchor samples and comparing their cosine similarities with the corresponding bit vectors. In contrast, verification in the black-box setting becomes more challenging under this shift toward *latent watermarking*. The latent alignment introduced at layer L propagates through the model, creating a subtle yet consistent statistical bias in the output logits.

While this bias is too small to alter the arg max prediction, it remains detectable through careful statistical analysis.

Our black-box verification mechanism (Section 4.3) is specifically designed to detect this effect. By restricting attention to a small set of *sentinel tokens* and using a paired-difference estimation against a pre-recorded signature, we eliminate semantic noise and isolate the latent bias. The subsequent Bayesian reanchoring procedure (Section 4.3.2) further tracks this bias under fine-tuning or distillation drift, enabling reliable recovery of the embedded signature even after substantial model modification.

4. Detailed Methodology

4.1. Watermark Injection via Model Editing

We insert an N -bit watermark into LLMs by leveraging ME techniques to align the latent representations of selected anchor samples with vectors that encode the corresponding bit information. Each anchor sample is assigned a watermark bit of either 0 or 1, and two orthogonal vectors are constructed to represent these bit values. A specific bit is then encoded through a controlled local update applied to the hidden representation of the chosen *subject token* within the anchor sample. The associated *object* remains unaffected by the update, which ensures that the model’s original functional behavior is preserved.

Setup and Bit Allocation. For an N -bit watermark, we first sample N factual triplets as anchor samples:

$$\mathcal{D}_{\text{anchor}} = \{(s_i, r_i, o_i)\}_{i=1}^N. \quad (6)$$

We then randomly assign a single bit $b_i \in \{0, 1\}$ to each anchor sample, thereby encoding an N -bit watermark.

For anchor triplet selection, we choose samples on which the model already demonstrates *high prediction confidence*. Specifically, a desired anchor triplet satisfies the condition $P_W(o_i | s_i, r_i) > \tau_a$, where W denotes the model to be watermarked and τ_a is a predefined confidence threshold typically set close to 1 (e.g., 0.9). This selection promotes a more stable optimization process during watermark embedding, as the objective focuses on aligning the anchor representation with its corresponding bit vector rather than learning the underlying factual mapping itself. We clarify that this requirement on anchor samples does not make them less stealthy. In practice, an anchor sample can be constructed by fixing the subject and relation while sampling the most probable object from the model’s vocabulary.

Bit Vector Construction. For each bit b_i , we generate two orthogonal unit vectors $[v_0^{(i)}, v_1^{(i)}]$ representing the binary codes $\{0, 1\}$, respectively. We first initialize $v_0^{(i)}$ and $v_1^{(i)}$ as random vectors drawn from a standard normal distribution, and then orthogonalize them using the Gram–Schmidt process to ensure orthogonality. Specifically, let d_L denote the hidden dimension corresponding to the hidden states of the inserted layer L .

$$v_0^{(i)} = \frac{n_0}{\|n_0\|_2}, \quad v_1^{(i)} = \frac{n_1 - (n_1^\top v_0^{(i)})v_0^{(i)}}{\|n_1 - (n_1^\top v_0^{(i)})v_0^{(i)}\|_2}, \quad (7)$$

where $n_0, n_1 \sim \mathcal{N}(0, I_{d_L})$. Thus, encoding a bit b_i into an LLM corresponds to aligning $v_{b_i}^{(i)}$ with the hidden representation of the subject token of a specific anchor sample.

Subject-Level Alignment via Model Editing. We proceed to align the hidden representation of each anchor sample with the corresponding bit vector. For each triplet (s_i, r_i, o_i) , we locate the hidden representation of the *last subject token* $h_L(s_i)$ at layer L . Instead of directly adding a fixed bit direction, we optimize an offset δ_i^L such that the updated representation $h'_L(s_i) = h_L(s_i) + \delta_i^L$ is maximally correlated with its designated bit vector while remaining orthogonal to all other bit vectors through distributional matching. Meanwhile, the optimization is constrained to preserve the model’s original factual prediction, ensuring that the watermark injection does not alter the model’s behavior. We demonstrate the alignment process in Figure 2 (a).

Bit-Space Construction. Inserting an N -bit watermark involves constructing $2N$ orthogonal bit vectors $\{v_0^{(1)}, v_1^{(1)}, \dots, v_0^{(N)}, v_1^{(N)}\}$, where each pair $(v_0^{(i)}, v_1^{(i)})$ represents the binary codes $\{0, 1\}$ for bit i . For the entire watermark sequence (b_1, \dots, b_N) , the i -th anchor sample is assigned the target bit b_i . We then transform the assigned i -th bit into a one-hot target vector $y_i \in \mathbb{R}^{2N}$, defined as:

$$y_i[j] = \begin{cases} 1, & \text{if } j = 2i - 1 \text{ and } b_i = 0, \\ 1, & \text{if } j = 2i \text{ and } b_i = 1, \\ 0, & \text{otherwise.} \end{cases} \quad (8)$$

where $y_i[j] = 1$ stands for the i -th anchor sample being assigned with the j -th bit vector.

Alignment Optimization. We compute the cosine similarity between the updated embedding and all $2N$ bit vectors for the i -th anchor sample as

$$p_i = \text{softmax}([\cos(h_L(s_i) + \delta_i^L, v_0^{(1)}), \dots, \cos(h_L(s_i) + \delta_i^L, v_1^{(N)})]). \quad (9)$$

We then minimize the divergence between p_i and y_i :

$$\delta^* = \arg \min_{\delta_i^L} \left[-\log P_\theta(o_i | s_i, r_i; h_L + \delta_i^L) \right] \quad (10)$$

$$+ \lambda_{\text{KL}} \text{KL}(y_i \| p_i) + \lambda_{\text{MSE}} \|p_i - y_i\|_2^2, \quad (11)$$

where the first term preserves the model’s prediction. We guide the embedding’s cosine similarity distribution toward the one-hot bit assignment by minimizing the Kullback–Leibler (KL) divergence between p_i and y_i . Since the KL divergence primarily captures distributional differences, we strengthen the alignment by minimizing the mean squared error (MSE) between p_i and y_i . The hyperparameters λ_{KL} and λ_{MSE} balance between these two objectives.

Parameter Update. After obtaining the optimized offset $\{\delta_i\}_{i=1}^N$ for all anchor samples, we compute their corresponding key embeddings $\{k_i\}_{i=1}^{N_t}$ from the last subject tokens. Following the closed-form formulation of ME [35],

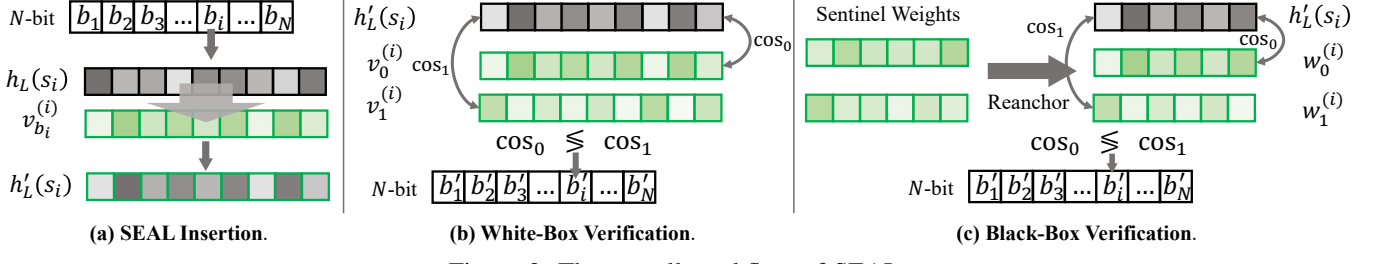


Figure 2: The overall workflow of SEAL.

the final parameter update Δ_L at layer L is derived by solving the following linear system:

$$\Delta_L \left(C_p + \sum_{i=1}^N k_i k_i^\top \right) = \sum_{i=1}^N \delta_i^L k_i^\top, \quad (12)$$

where $C_p = \lambda \mathbb{E}_{k_p} [k_p k_p^\top]$ approximates the covariance of preserved knowledge, and λ controls the balance between preserving existing knowledge and encoding new bits. The closed-form solution is then

$$\Delta_L = \left(\sum_{i=1}^N \delta_i^L k_i^\top \right) \left(C_p + \sum_{i=1}^N k_i k_i^\top \right)^{-1}. \quad (13)$$

Finally, the model parameters are updated as $W_L^{\text{new}} = W_L^{\text{old}} + \Delta_L$, where the watermark is encoded within the hidden representation subspace of the MLP modules.

The updates can also be distributed across multiple candidate layers to further enhance robustness and minimize the overall impact on the model. This is achieved by sequentially updating all selected layers from shallow to deep. For each layer ℓ in all candidate layers, we compute the corresponding update Δ_ℓ^ℓ following Equation 13 by downscaling the optimized offset δ_i^ℓ in each layer with λ_ℓ , that is, $\delta_i^\ell = \delta_i^L / \lambda_\ell$, where λ_ℓ decreases with layer depth and equals 1 for the final layer [35]. We discuss the details of different layer selection strategies in Section 6.5. Overall, this global update embeds the optimized watermark bits into the model’s memory while maintaining high fidelity to its original functionality.

4.2. White-Box Verification

As shown in Figure 2 (b), we can directly inspect the hidden representations of the predefined anchor samples to verify the embedded watermark bits under white-box access.

Direct Embedding Inspection. For each anchor sample (s_i, r_i, o_i) at the target layer L , we extract the hidden representation of the last subject token, $h_L(s_i)$, and compute its cosine similarities with the two bit vectors $\{v_0^{(i)}, v_1^{(i)}\}$ representing the binary codes $\{0, 1\}$:

$$\cos_0 = \cos(h_L(s_i), v_0^{(i)}), \quad \cos_1 = \cos(h_L(s_i), v_1^{(i)}). \quad (14)$$

The recovered bit \hat{b}_i is set to 1 if $\cos_1 > \cos_0$, and 0 otherwise. By performing this comparison across all anchor

samples, we can recover the complete watermark bit sequence $\hat{b} = (\hat{b}_1, \dots, \hat{b}_N)$.

4.3. Black-Box Verification

In the black-box setting, the defender has no access to the model’s internal parameters or hidden representations and can only query its output logits. To verify the embedded watermark under such constraints, we first examine how each bit vector influences the output logits after watermark insertion. The resulting logit pattern is then treated as a unique identifier for subsequent verification.

Counteract with Adversaries. When the model is modified by fine-tuning, distillation, or other adversarial operations that aim to remove the watermark, the corresponding logit signatures may drift. To counteract this effect, we introduce a *Bayesian reanchoring* procedure that adaptively compensates for model drift and restores the alignment between the bit vectors and their reference signatures based on precomputed information before the watermarked model is deployed. Notice that we do not assume the defender has knowledge of the exact modification process applied to the model. Instead, we only assume access to a small set of reference triplets that are different from the anchor samples used during watermark insertion.

We proceed to introduce the details of our black-box verification framework from three key components: (1) pre-computed signatures before deployment, (2) Bayesian reanchoring procedure to mitigate model drift, and (3) bit-wise logit comparison for final verification. We demonstrate the verification process in Figure 2 (c).

4.3.1. Precomputed Bit Signatures. Before deploying the watermarked model, we precompute the influence of each bit vector on the output logits to obtain its corresponding *bit signature*. These signatures act as practical approximations of the bit vectors in the logit space and can serve as reference points for subsequent black-box verification. To estimate the influence of each bit vector, we collect an auxiliary set of reference triplets $\mathcal{D}_{\text{ref}} = \{(s_k, r_k, o_k)\}_{k=1}^K$. For each bit vector v_{b_i} , we simulate the watermark insertion process by slightly perturbing the hidden state of the last subject token in \mathcal{D}_{ref} using v_{b_i} , and then observe the induced changes in the output logits. Specifically, at the target layer L , the hidden state of the last subject token is perturbed as

$$h'_L(s_k) = h_L(s_k) + \eta v_{b_i}, \quad (15)$$

where η is a small scaling factor. The perturbed hidden state is then projected to the vocabulary logits by the rest part of the LLM $f(\cdot)$. The influence of v_{b_i} on the output logits is estimated by averaging the logit differences across all reference triplets:

$$\frac{1}{K} \sum_{k=1}^K (f(h'_L(s_k)) - f(h_L(s_k))) \quad (16)$$

$$= \frac{1}{K} \sum_{k=1}^K (f(h_L(s_k) + \eta v_{b_i}) - f(h_L(s_k))) \approx f(v_{b_i}) \quad (17)$$

Here, the scaling factor η is set sufficiently small such that the perturbation lies within the locally linear regime of the logit mapping. Under this assumption, the change of output logits can be approximated by a linear response to the injected direction v_{b_i} , allowing us to estimate the influence of each bit vector as $f(v_{b_i})$.

We then select a set of representative tokens that exhibit the highest logit responses with respect to v_{b_i} , referred to as the *sentinel tokens*, denoted by $\mathcal{T} = \{t_1, \dots, t_m\}$. Their projection responses are recorded as

$$w_{\text{sig}}^{(i)} = \{f(v_{b_i})[t_j] | j = 1, \dots, m\} \quad (18)$$

where $f(v_{b_i})[t_j]$ denotes the logit of the j -th sentinel token for the bit vector v_{b_i} . Each $w_{\text{sig}}^{(i)}$ serves as a unique reference signature for the i -th bit within the logit space, providing a stable basis for black-box verification in later stages.

4.3.2. Black-Box Bayesian Reanchoring. An adversary’s attempt to remove the watermark through fine-tuning or knowledge distillation may cause the bit-vector direction v_b to drift, thereby shifting its projection on the sentinel logits. To correct this drift and recover the effective sentinel weights under the deployed model, we propose a *Bayesian reanchoring* procedure. This process first estimates the logit drift between the original watermarked model and the deployed model using the same set of reference triplets \mathcal{D}_{ref} , and then infers the posterior change within the logit subspace to reconstruct the effective sentinel weights.

Estimating Logit Drift. To estimate the logit drift, we first record the sentinel logits of the watermarked model $f^W(\cdot)$ on the reference dataset \mathcal{D}_{ref} :

$$\mathcal{L}_k^W = f^W(s_k)[\mathcal{T}] = S_k + w_{\text{sig}} + \epsilon_k^0, \quad (19)$$

where S_k denotes the prompt-dependent semantic term.

For the deployed model $f^D(\cdot)$, the defender can query it with the same dataset \mathcal{D}_{ref} and collect the logits restricted to the sentinel token set \mathcal{T} :

$$\mathcal{L}_k^D = f^D(s_k)[\mathcal{T}] = S_k + w^* + \epsilon_k, \quad (20)$$

where $w^* \in \mathbb{R}^{|\mathcal{T}|}$ denotes the latent sentinel-weight vector.

To eliminate the semantic component S_k , we compute the paired difference between the two models’ logits:

$$\Delta \mathcal{L}_k = \mathcal{L}_k^D - \mathcal{L}_k^W = (w^* - w_{\text{sig}}) + (\epsilon_k - \epsilon_k^0), \quad (21)$$

which yields an unbiased estimate of the drift between the deployed and reference signatures. We summarize these samples via their empirical mean and covariance:

$$\mu_\Delta = \mathbb{E}[\Delta \mathcal{L}], \quad \Sigma_\Delta = \text{Cov}(\Delta \mathcal{L}), \quad (22)$$

which characterize the average drift and the variation within the sentinel logit subspace.

Bayesian Reanchoring. To correct the observed logit drift and recover the effective sentinel weights under the deployed model, we perform *Bayesian reanchoring* based on the precomputed sentinel signatures.

Assuming a Gaussian prior $p(w) = \mathcal{N}(w_{\text{sig}}, \lambda^{-1}I)$ and a Gaussian likelihood $p(\mu_\Delta | w) = \mathcal{N}(w - w_{\text{sig}}, \rho \Sigma_\Delta)$, the posterior mean admits the closed-form solution:

$$w^* = (\rho \Sigma_\Delta + \lambda I)^{-1} (w_{\text{sig}} + P \mu_\Delta + \lambda P w_{\text{sig}}), \quad (23)$$

where $P = I - \frac{11^\top}{m}$ removes uniform offsets from the estimated directions. The resulting posterior mean w^* denotes the reanchored sentinel weights under the deployed model, effectively compensating for model drift. We leave the detailed derivation in the Appendix B.

4.3.3. Bit-Wise Verification. With reanchored sentinel weights $\{w_0^{(i)}, w_1^{(i)}\}$, we can verify the watermark by comparing the logit responses of the anchor samples to the reanchored sentinel weights.

For each anchor sample (s_i, r_i, o_i) , we collect the sentinel logits of the subject token of s_i :

$$\mathcal{L}_i = f^D(s_i)[\mathcal{T}] \in \mathbb{R}^{|\mathcal{T}|}. \quad (24)$$

We then compute inner products with the two weights:

$$s_0 = \langle \mathcal{L}_i, w_0^{(i)} \rangle, \quad s_1 = \langle \mathcal{L}_i, w_1^{(i)} \rangle, \quad (25)$$

and determine the recovered bit \hat{b}_i as 1 if $s_1 > s_0$, and 0 otherwise. Repeating this for all anchor samples yields the recovered bit sequence $\hat{b} = (\hat{b}_1, \dots, \hat{b}_N)$.

4.4. Security and Practicality Explanation

4.4.1. Security Assumptions. Following the above technical pipeline, we now summarize the security assumption and information visibility of SEAL. By clarifying these, we better explain its security strength, even in front of advanced, “knowledgeable” attackers (see below).

Defender Side. The defender privately maintains the following information: (1) a set of N anchor samples $\mathcal{A} = \{(s_i, r_i, o_i)\}_{i=1}^N$, which serve as secret semantic carriers for watermark embedding; (2) a corresponding set of $2N$ orthogonal bit vectors $\mathcal{V} = \{v_0^{(i)}, v_1^{(i)}\}_{i=1}^N$ that define the subspace encoding of each bit; and (3) for black-box verification purposes, notice a sentinel token set \mathcal{T} and reference dataset \mathcal{D}_{ref} for Bayesian reanchoring are generated prior to deployment; these are also kept secret. These elements collectively constitute the defender’s “secret key” and are neither disclosed nor inferable by adversaries.

Public Information. The embedding and verification algorithms of SEAL, including the training objectives, loss

functions, and reanchoring procedures, are *public* by design. However, adversaries do not have access to the exact anchor samples or bit vectors that define the encoded subspace.

Adversary Knowledge. Although the SEAL procedure is publicly available, ordinary attackers *do not* have access to the specific configuration, such as the exact layers for watermark embedding. This is reasonable, as such implementation details are rarely disclosed in practice, and modern LLMs often have complex architectures with numerous layers, making exhaustive guessing impractical. Given that, we also consider more knowledgeable attackers who are aware of the general SEAL mechanism and may even infer the target layer used for watermark injection. This represents a realistic scenario in which adversaries can deduce partial implementation details from public information. Based on the results (Section 6.5), different layers manifest distinct support on watermarking effectiveness. Thus, we assume that knowledgeable, advanced attackers may identify certain layers that have a high chance of containing watermarks (e.g., those “deep” layers). We name these attackers as “knowledgeable attackers” and assess them in Section 7.

4.4.2. Usage in Practice. We now discuss using SEAL in practice for lineage identification, ownership verification, and model deployment.

Lineage Identification. Model lineage is identified by comparing the cosine similarity between the recovered bit sequences of two models. A high similarity score indicates that the two models are derived from the same watermarked source, without requiring an exact bit-wise match.

Ownership Verification. After recovering $\hat{b} \in \{0, 1\}^N$ using either white-box or black-box verification methods, the defender can compare \hat{b} with the registered signature b^* and compute the *bit error rate (BER)* as

$$\text{BER} = \frac{1}{N} \sum_{i=1}^N \mathbb{I}[\hat{b}_i \neq b_i^*]. \quad (26)$$

Ownership is claimed when $\text{BER} < \tau$, where τ is a predefined verification threshold. A smaller τ leads to a negligible false positive rate (FPR) in ownership claims, since the probability that a random watermark coincidentally matches the defender’s signature decreases *exponentially* with N . For example, when $\tau = 0$, a 64-bit watermark yields an FPR of 2^{-64} , which is practically zero for IP-related applications. Therefore, in IP protection scenarios (which are often high-stake and legally binding), we conservatively adopt an *exact-match* criterion (i.e., $\tau = 0$) to avoid ambiguity in ownership claims. Our experiments in Section 6.2 demonstrate that SEAL achieves near-zero BER, enabling deterministic verification without relying on probabilistic thresholds.

In practice, bit errors may occur due to statistical randomness or even hardware faults. To mitigate this, we further discuss incorporating error-correcting codes (ECC) [46], [47], [48] into the watermark encoding to tolerate minor bit corruption in Appendix C.

Deploying SEAL. To deploy SEAL, the defender generates and stores $2N$ bit vectors and their corresponding anchor

set for each model instance prior to release. This one-time cost is negligible compared to model pretraining or fine-tuning. During verification, SEAL only requires access to hidden representations (for white-box verification) or output logits (for black-box verification). Consequently, the framework is fully compatible with API-based verification, where access to model logits is commonly available in many LLM APIs [44], [45], and introduces minimal computational overhead.

5. Evaluation Setup and Configuration

Evaluation Setup. We evaluate our method on six representative LLMs: LLaMA2-7B [3], LLaMA3-8B [4], Qwen2.5-7B [49], Qwen2.5-14B [49], Mistral-7B [50], and DeepSeek-Chat-7B [51]. To assess robustness, we consider five categories of model-level attacks that aim to remove the embedded watermark or disrupt fingerprint extraction: SFT [19], PEFT [24], [25], DT [26], [27], [28], QT [29], [30], [31], and MM [32], [33], [34].

For SFT attacks, we perform full-parameter fine-tuning on two public instruction-following datasets, Alpaca [52] and UltraChat [53]. For PEFT attacks, we inject LoRA adapters into the model and fine-tune only the inserted low-rank parameters. For distillation attacks, we assume a setting where the watermark is injected into a student model while the adversary distills knowledge from a larger or fine-tuned teacher model into the watermarked student [54], [55], [56].

Notice that, based on our experiments, modification on those deeper layers manifests poorer influence on the output logits. Thus, as a reasonable assumption, we consider attackers tend to target those “shallow” layers for modification to maximize the impact on model behavior. Hence, without loss of generality, for these attacks, we assume the attacker targets layers (5, 6, 7, 8, 9, 10) by default. We further discuss the impact of this assumption in Section 7.

To simulate quantization, we apply symmetric per-tensor fake quantization, where each floating-point weight tensor is scaled by its maximum absolute value and projected onto a uniform n -bit integer grid before being dequantized back to floating point. We set $n = 8$ in all experiments [57]. Finally, for model-merging attacks, we linearly interpolate the parameters of the watermarked model and its fine-tuned counterpart for the merged model $\theta'_{\text{merged}} = \alpha \theta'_{\text{watermarked}} + (1 - \alpha) \theta'_{\text{fine-tuned}}$ where $\alpha = 0.7$ in all experiments.

Baseline Methods. We compare our approach against a comprehensive set of existing fingerprinting and watermarking methods. Among them, Gradient [10], [58], Huref [38], Reef [59], and PDF [60] require *white-box* access to the model parameters. In contrast, LLMMMap [13], MET [11], SEF [10], and Trap [12] operate under the *black-box* setting, where only model outputs or logits are accessible. We further include backdoor-based watermarking baselines, namely SFP [61] and IF [19]. For IF, we evaluate two variants: IF-sft, which fine-tunes transformer layers using full-parameter SFT, and IF-emb, which fine-tunes only the embedding layer.

TABLE 2: Model lineage identification performance of SEAL and baselines under white-box and black-box settings across six LLMs. SEAL(W) and SEAL(B) denote the white-box and black-box variants.

Model	Metric	White-box					Black-box							
		Gradient	Huref	Reef	PDF	SEAL(W)	LLMMap	MET	SEF	Trap	SFP	IF-sft	IF-emb	SEAL(B)
LLaMA2-7B	AUC \uparrow	0.53 \pm 0.01	1.00 \pm 0.00	1.00 \pm 0.02	1.00 \pm 0.00	1.00 \pm 0.00	0.30 \pm 0.01	0.47 \pm 0.01	0.28 \pm 0.01	0.44 \pm 0.03	0.67 \pm 0.04	0.50 \pm 0.00	0.50 \pm 0.00	1.00 \pm 0.00
	pAUC \uparrow	0.33 \pm 0.01	1.00 \pm 0.00	1.00 \pm 0.02	1.00 \pm 0.00	1.00 \pm 0.00	0.17 \pm 0.01	0.00 \pm 0.00	0.00 \pm 0.00	0.33 \pm 0.01	0.33 \pm 0.03	0.00 \pm 0.00	0.00 \pm 0.00	1.00 \pm 0.00
	MD \uparrow	0.25 \pm 0.03	1.84 \pm 0.00	1.91 \pm 0.06	1.52 \pm 0.00	1.92 \pm 0.01	0.70 \pm 0.02	0.87 \pm 0.04	1.34 \pm 0.01	1.41 \pm 0.07	0.86 \pm 0.04	0.00 \pm 0.00	0.00 \pm 0.00	1.89 \pm 0.02
Qwen2.5-7B	AUC \uparrow	0.97 \pm 0.00	1.00 \pm 0.00	1.00 \pm 0.02	1.00 \pm 0.00	1.00 \pm 0.00	0.67 \pm 0.02	0.18 \pm 0.01	0.67 \pm 0.03	0.50 \pm 0.02	0.50 \pm 0.02	0.50 \pm 0.00	0.50 \pm 0.00	1.00 \pm 0.00
	pAUC \uparrow	0.83 \pm 0.01	1.00 \pm 0.00	1.00 \pm 0.01	1.00 \pm 0.00	1.00 \pm 0.00	0.67 \pm 0.01	0.00 \pm 0.00	0.67 \pm 0.02	0.00 \pm 0.00	0.00 \pm 0.00	0.00 \pm 0.00	0.00 \pm 0.00	1.00 \pm 0.00
	MD \uparrow	1.54 \pm 0.02	1.91 \pm 0.00	1.71 \pm 0.05	1.79 \pm 0.00	1.92 \pm 0.02	0.15 \pm 0.01	1.34 \pm 0.03	1.50 \pm 0.04	0.00 \pm 0.00	0.00 \pm 0.00	0.00 \pm 0.00	0.00 \pm 0.00	1.91 \pm 0.01
LLaMA3-8B	AUC \uparrow	0.94 \pm 0.02	1.00 \pm 0.00	1.00 \pm 0.02	0.94 \pm 0.00	1.00 \pm 0.00	0.33 \pm 0.01	0.67 \pm 0.02	0.28 \pm 0.02	0.33 \pm 0.02	0.58 \pm 0.02	0.50 \pm 0.00	0.50 \pm 0.00	1.00 \pm 0.00
	pAUC \uparrow	0.67 \pm 0.01	1.00 \pm 0.00	1.00 \pm 0.02	0.67 \pm 0.00	1.00 \pm 0.00	0.33 \pm 0.02	0.33 \pm 0.01	0.00 \pm 0.00	0.33 \pm 0.01	0.17 \pm 0.01	0.00 \pm 0.00	0.00 \pm 0.00	1.00 \pm 0.00
	MD \uparrow	1.51 \pm 0.00	1.90 \pm 0.00	1.85 \pm 0.06	1.52 \pm 0.00	1.91 \pm 0.02	0.58 \pm 0.03	0.86 \pm 0.03	1.43 \pm 0.03	1.90 \pm 0.04	0.58 \pm 0.03	0.00 \pm 0.00	0.00 \pm 0.00	1.92 \pm 0.01
Mistral-7B	AUC \uparrow	1.00 \pm 0.01	1.00 \pm 0.00	1.00 \pm 0.02	1.00 \pm 0.00	1.00 \pm 0.00	0.00 \pm 0.00	0.25 \pm 0.01	0.00 \pm 0.00	0.42 \pm 0.02	0.58 \pm 0.02	0.50 \pm 0.00	0.50 \pm 0.00	1.00 \pm 0.00
	pAUC \uparrow	1.00 \pm 0.00	1.00 \pm 0.00	1.00 \pm 0.01	1.00 \pm 0.00	1.00 \pm 0.00	0.00 \pm 0.00	0.00 \pm 0.00	0.00 \pm 0.00	0.17 \pm 0.02	0.00 \pm 0.00	0.00 \pm 0.00	0.00 \pm 0.00	1.00 \pm 0.00
	MD \uparrow	1.58 \pm 0.00	1.91 \pm 0.00	1.87 \pm 0.04	1.76 \pm 0.00	1.94 \pm 0.01	1.55 \pm 0.01	1.11 \pm 0.03	1.90 \pm 0.02	0.57 \pm 0.03	0.58 \pm 0.04	0.00 \pm 0.00	0.00 \pm 0.00	1.90 \pm 0.00
Deepseek-7B	AUC \uparrow	0.80 \pm 0.01	1.00 \pm 0.00	1.00 \pm 0.02	1.00 \pm 0.00	1.00 \pm 0.00	0.00 \pm 0.00	0.28 \pm 0.01	0.00 \pm 0.00	0.50 \pm 0.03	0.50 \pm 0.02	0.50 \pm 0.00	0.50 \pm 0.00	1.00 \pm 0.00
	pAUC \uparrow	0.50 \pm 0.02	1.00 \pm 0.00	1.00 \pm 0.01	1.00 \pm 0.00	1.00 \pm 0.00	0.00 \pm 0.00	1.00 \pm 0.00						
	MD \uparrow	0.97 \pm 0.00	1.88 \pm 0.00	1.91 \pm 0.07	1.68 \pm 0.00	1.91 \pm 0.01	1.52 \pm 0.04	1.55 \pm 0.03	1.84 \pm 0.02	0.00 \pm 0.00	0.00 \pm 0.00	0.00 \pm 0.00	0.00 \pm 0.00	1.89 \pm 0.01
Qwen2.5-14B	AUC \uparrow	1.00 \pm 0.00	1.00 \pm 0.00	1.00 \pm 0.00	1.00 \pm 0.00	1.00 \pm 0.00	0.31 \pm 0.02	0.42 \pm 0.02	0.50 \pm 0.03	0.28 \pm 0.02	0.50 \pm 0.01	0.50 \pm 0.00	0.50 \pm 0.00	1.00 \pm 0.00
	pAUC \uparrow	1.00 \pm 0.01	1.00 \pm 0.00	1.00 \pm 0.00	1.00 \pm 0.00	1.00 \pm 0.00	0.17 \pm 0.01	0.00 \pm 0.00	0.50 \pm 0.02	0.00 \pm 0.00	0.00 \pm 0.00	0.00 \pm 0.00	0.00 \pm 0.00	1.00 \pm 0.00
	MD \uparrow	1.53 \pm 0.02	1.88 \pm 0.00	1.90 \pm 0.00	1.65 \pm 0.00	1.92 \pm 0.01	0.53 \pm 0.02	0.58 \pm 0.02	0.39 \pm 0.03	1.42 \pm 0.03	0.00 \pm 0.00	0.00 \pm 0.00	0.00 \pm 0.00	1.89 \pm 0.00

Evaluation Metrics. We first evaluate the effectiveness of identifying model lineage. For fair comparison with existing fingerprinting methods, we adopt the same evaluation metrics (AUC, pAUC, and MD) commonly used in prior literature [10]. A higher AUC, pAUC, or MD indicates stronger discriminative power. We refer to Appendix D for more details. We then compute these metrics for each model when compared against others, as summarized in Table 10.

To further evaluate the characteristics of our watermarking approach, we design the following metrics to assess the multi-bit watermarking capacity:

- **Bit Error Rate (BER).** The proportion of incorrectly recovered bits relative to the originally embedded bits. Lower BER denotes more reliable watermark extraction. We report all BER values as percentages (%).
- **Bit Separability (BSE).** The average gap between a watermarked bit vector’s similarity to its corresponding versus non-corresponding original bit vectors. Higher BSE implies stronger bit separability.
- **Bit Stability (BST).** The standard deviation of the similarity scores between watermarked bits and their original counterparts across repeated extractions. Lower BST implies greater robustness and stability of the watermark.

SEAL Settings. We embed multi-bit watermarks into the model and evaluate under both *white-box* and *black-box* settings. By default, each model is embedded with a 64-bit watermark. We also extend the evaluation to different bit lengths, including 32, 64, 128, 256, 512, and 1024 bits. For watermark embedding, we select samples from the *Counter-Fact* dataset [62]. Specifically, we select samples on which the model exhibits high prediction confidence, enabling a more stable optimization during watermark embedding. We further discuss this choice in Section 6.5.

6. Evaluation

We organize our evaluation around the following five research questions (RQs): **RQ1:** How effective is SEAL in identifying model lineage compared with existing methods? **RQ2:** How effective is SEAL in extracting watermarks under various attack behaviors? **RQ3:** How harmless is SEAL to the model’s original performance and utility? **RQ4:** How does SEAL perform in watermark extraction across different bit lengths, in terms of time efficiency and GPU usage? **RQ5:** How do different hyperparameter settings affect the effectiveness of SEAL in watermark extraction?

6.1. RQ1: Model Lineage Identification

We first evaluate the **Effectiveness** of SEAL in identifying derivative models from independent ones, in comparison with existing fingerprinting methods.

SEAL Effectively Identifies Model Lineage Across Different LLMs. As summarized in Table 2, SEAL consistently achieves superior performance in distinguishing derivative models from independent ones. Across all evaluation settings, SEAL attains perfect AUC and pAUC scores of 1.00, and also achieves the highest MD across all LLMs, indicating that the extracted features are highly separable for different model lineages. These results demonstrate that SEAL achieves state-of-the-art effectiveness in model lineage identification.

SEAL Maintains High Lineage Identification Accuracy in Both White-Box and Black-Box Scenarios. As shown in Table 2, SEAL remains highly effective in identifying model lineage even under the black-box setting, where only query access or output logits are available. Across all six LLMs, SEAL achieves perfect AUC and pAUC scores of 1.00 when distinguishing derivative models from independent ones. In contrast, most existing fingerprinting methods fail to effectively identify model lineage, performing close to

random guessing with AUC values around 0.5. Similarly, backdoor-based watermarking methods such as SFP and IF also fail to maintain accuracy, as their injected backdoor behaviors are easily removed through fine-tuning, rendering their lineage identification capabilities fragile.

In the white-box setting, where full model parameters are accessible, existing fingerprinting methods demonstrate promising performance in lineage identification. Among them, Huref, Reef, and PDF achieve near-perfect AUC and pAUC scores close to 1.00, while Gradient exhibits limited adaptability across different LLMs, achieving only 0.53 AUC in distinguishing derivative models of LLaMA2-7B from other independent models. Despite the competitive performance of these methods, SEAL consistently maintains perfect AUC and pAUC scores of 1.00, along with the highest MD across all LLMs, indicating superior separability between derivative and independent models.

Overall, these results highlight SEAL’s superior effectiveness in model lineage identification, particularly under black-box conditions where existing methods fail to generalize or retain reliability.

6.2. RQ2: Multi-Bit Watermark Extraction

Existing fingerprinting and watermarking methods are usually limited to identifying model lineage or embedding a single-bit piece of information. This limitation constrains their applicability for sophisticated multi-bit ownership verification, which requires embedding and extracting multi-bit information. We therefore evaluate the **Effectiveness** of SEAL in extracting multi-bit watermarks under various attack scenarios.

TABLE 3: Multi-bit watermark extraction performance of SEAL under different attack behaviors.

Evaluation	Bits	Metrics	No attack	SFT	PEFT	DT	QT	MM
White-box	64	BER \downarrow	0.06 \pm 1.25	0.00 \pm 0.00	0.63 \pm 1.25	0.06 \pm 1.25	0.00 \pm 0.00	0.00 \pm 0.00
		BSE \uparrow	0.04 \pm 0.09	0.01 \pm 0.03	0.03 \pm 0.09	0.05 \pm 0.08	0.05 \pm 0.10	0.02 \pm 0.06
		BST \downarrow	0.76 \pm 0.05	0.49 \pm 0.16	0.67 \pm 0.03	0.62 \pm 0.13	0.72 \pm 0.05	0.38 \pm 0.11
	128	BER \downarrow	0.00 \pm 0.00	0.52 \pm 1.36	0.00 \pm 0.00	0.07 \pm 0.21	0.00 \pm 0.00	0.95 \pm 0.42
		BSE \uparrow	0.02 \pm 0.06	0.01 \pm 0.06	0.02 \pm 0.07	0.00 \pm 0.05	0.03 \pm 0.09	0.02 \pm 0.06
		BST \downarrow	0.75 \pm 0.05	0.50 \pm 0.19	0.68 \pm 0.02	0.56 \pm 0.15	0.72 \pm 0.05	0.39 \pm 0.11
	256	BER \downarrow	0.00 \pm 0.00	0.15 \pm 0.27	0.00 \pm 0.00	0.10 \pm 0.17	0.36 \pm 0.40	0.39 \pm 0.55
		BSE \uparrow	0.02 \pm 0.02	0.01 \pm 0.01	0.02 \pm 0.01	0.01 \pm 0.01	0.04 \pm 0.01	0.02 \pm 0.01
		BST \downarrow	0.75 \pm 0.06	0.43 \pm 0.21	0.60 \pm 0.12	0.53 \pm 0.19	0.68 \pm 0.03	0.27 \pm 0.10
	512	BER \downarrow	0.08 \pm 0.15	0.16 \pm 0.09	0.08 \pm 0.16	0.12 \pm 0.16	0.09 \pm 0.16	0.15 \pm 0.25
		BSE \uparrow	0.02 \pm 0.02	0.01 \pm 0.01	0.02 \pm 0.03	0.02 \pm 0.03	0.01 \pm 0.01	0.01 \pm 0.03
		BST \downarrow	0.75 \pm 0.04	0.46 \pm 0.15	0.64 \pm 0.07	0.54 \pm 0.23	0.70 \pm 0.03	0.38 \pm 0.13
Black-box	64	BER \downarrow	0.31 \pm 0.63	1.03 \pm 1.52	0.16 \pm 0.47	1.09 \pm 2.80	0.26 \pm 0.58	2.08 \pm 4.00
		BSE \uparrow	0.02 \pm 0.01	0.01 \pm 0.01	0.01 \pm 0.01	0.01 \pm 0.01	0.00 \pm 0.00	0.01 \pm 0.01
		BST \downarrow	0.00 \pm 0.00	0.00 \pm 0.00	0.00 \pm 0.00	0.00 \pm 0.00	0.00 \pm 0.00	0.00 \pm 0.00
	128	BER \downarrow	0.00 \pm 0.00	1.13 \pm 2.81	0.08 \pm 0.23	1.34 \pm 1.49	0.16 \pm 0.31	4.06 \pm 3.72
		BSE \uparrow	0.02 \pm 0.01	0.01 \pm 0.01	0.01 \pm 0.01	0.02 \pm 0.01	0.01 \pm 0.01	0.01 \pm 0.01
		BST \downarrow	0.00 \pm 0.00	0.00 \pm 0.00	0.00 \pm 0.00	0.00 \pm 0.00	0.00 \pm 0.00	0.00 \pm 0.00
	256	BER \downarrow	0.09 \pm 0.16	1.51 \pm 3.95	1.21 \pm 1.09	1.53 \pm 2.17	0.19 \pm 0.33	4.10 \pm 2.35
		BSE \uparrow	0.01 \pm 0.00	0.01 \pm 0.00	0.02 \pm 0.01	0.02 \pm 0.01	0.01 \pm 0.01	0.02 \pm 0.02
		BST \downarrow	0.00 \pm 0.00	0.00 \pm 0.00	0.01 \pm 0.00	0.01 \pm 0.01	0.00 \pm 0.00	0.01 \pm 0.00
	512	BER \downarrow	0.04 \pm 0.08	1.68 \pm 2.27	1.26 \pm 1.21	2.65 \pm 3.27	0.24 \pm 0.25	2.75 \pm 2.38
		BSE \uparrow	0.02 \pm 0.02	0.02 \pm 0.01	0.02 \pm 0.01	0.02 \pm 0.02	0.02 \pm 0.01	0.02 \pm 0.02
		BST \downarrow	0.00 \pm 0.00	0.00 \pm 0.00	0.00 \pm 0.00	0.00 \pm 0.00	0.00 \pm 0.00	0.00 \pm 0.00

SEAL Effectively Extracts Multi-Bit Watermarks Under Various Attack Behaviors.

As shown in Table 3, SEAL effectively extracts watermarks of different bit lengths under all evaluated attack behaviors that attempt to remove the

embedded signals. Across all attack methods and bit lengths, SEAL achieves an average BER of 0.69%. Specifically, under SFT attacks, the error rate of the extracted watermarks remains below 1.51% across all configurations. SEAL demonstrates even stronger robustness against PEFT attacks, where the maximum BER is 1.21% when extracting 256-bit watermarks in the black-box setting, while the BER in all other cases remains close to zero. This is because PEFT updates cause slight changes to the model’s parameters compared to SFT updates. Quantization attacks have a negligible effect on the alignment between anchor samples and their corresponding bit vectors, with the highest observed BER of only 0.39%. Among all evaluated attacks, model merging poses the greatest challenge to extraction accuracy, as it linearly averages the watermarked model with another model. Despite this, SEAL still successfully extracts the embedded watermark bits, achieving a maximum BER of only 4.10% when extracting 256-bit watermarks in the black-box setting. These results demonstrate SEAL’s strong robustness against all evaluated attacks while maintaining accurate and reliable multi-bit watermark extraction.

SEAL Maintains Robustness in Both White-Box and Black-Box Scenarios. In Table 3, SEAL achieves nearly perfect extraction accuracy across all evaluated attack types, with the highest BER being only 0.95% in the white-box setting. In the black-box setting, attempts to remove the inserted watermarks are slightly more effective, but still fail to meaningfully affect the extraction accuracy. Under SFT attacks, SEAL attains an average BER of 0.17% in the white-box setting, while the average BER in the black-box setting increases slightly to 1.21%, which typically corresponds to only one or two incorrectly extracted bits out of a total of 128 or 256 bits. This minor increase in BER is expected, as the black-box setting provides only output logits, which are more sensitive to changes in model parameters. Nevertheless, SEAL demonstrates strong robustness against all evaluated attack types under both white-box and black-box conditions.

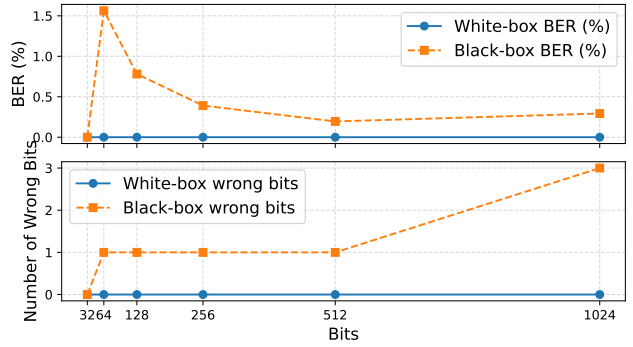


Figure 3: Scalability of SEAL in extracting multi-bit watermarks with increasing bit length under SFT attacks. We report the BER and the number of incorrectly extracted bits for each bit length.

SEAL Supports Reliable Multi-Bit Watermark Extraction up to 1024 Bits. We further examine the scalability

of SEAL in extracting multi-bit watermarks with increasing bit length under SFT attacks. As shown in Fig. 3, SEAL can reliably embed and extract up to 1024 watermark bits. Since SEAL achieves perfect extraction performance in the white-box setting, we focus our analysis on the black-box setting to evaluate scalability.

As observed, the number of incorrectly extracted bits remains largely stable as the total number of embedded bits increases. Specifically, no errors occur for 32-bit watermarks, while only one bit is extracted incorrectly when the total bit length increases to 64, 256, or 512. When extracting 1024 bits, the number of incorrectly extracted bits increases slightly to three. This results in an interesting trend in BER. It first increases to 1.56% at 64 bits and then decreases to 0.78% at 512 bits, as the number of incorrect bits remains nearly constant while the total embedded bits grow exponentially.

These results demonstrate SEAL’s strong scalability and robustness under increased embedding capacity. While SEAL can theoretically support longer bit sequences, we limit our experiments to 1024 bits due to practical considerations in real-world watermark verification, where shorter bit lengths are typically sufficient for copyright attribution.

6.3. RQ3: Fidelity of Injecting SEAL

We further evaluate the **Fidelity** of SEAL to examine whether watermark injection degrades the model’s original performance. Specifically, we compare the unmodified model with its watermarked counterparts embedded with varying numbers of verification bits across 15 downstream tasks, which cover a broad range of language understanding capabilities, including:

- **General Knowledge and Reasoning:** MMLU [63], BoolQ [64], Winogrande and WSC [65], COPA [66], PiQA [67], OpenBookQA [68] and ARC Challenge [69].
- **Sentence-level Understanding and Inference:** SST-2 [70], CoLA [71], MRPC [72], RTE and NLI [70].
- **Lexical and Contextual Semantics:** CB [73], WiC [74].

We report the mean and standard deviation of performance for three representative LLMs: LLaMA2-7B, LLaMA3-8B, and DeepSeek-Chat-7B. To examine the effect of watermark injection at different bit lengths on the models’ original performance, we compare the baseline models with their SEAL-watermarked counterparts, with the number of injected bits ranging from 64 to 512.

Injecting SEAL Preserves Model Performance. Table 4 summarizes the performance differences between the watermarked models and their original counterparts. As shown, injecting SEAL watermarks has only a negligible impact on downstream performance across all tasks and models, with the maximum average deviation being 0.058 and nearly all task-wise differences below 0.1. In particular, when injecting 64-bit watermarks, the performance of the watermarked models on general knowledge and reasoning benchmarks remains almost identical to that of the original models. Among the eight evaluated tasks, only MMLU and WSC exhibit

TABLE 4: Performance difference of injecting SEAL watermarks with different numbers of injected bits.

Metric	64 Bits	128 Bits	256 Bits	512 Bits
ARC	0.008±0.002	0.013±0.003	0.029±0.002	0.055±0.014
BoolQ	0.009±0.002	0.010±0.003	0.041±0.027	0.041±0.008
COPA	0.010±0.000	0.017±0.005	0.017±0.005	0.017±0.009
MMLU	0.045±0.023	0.064±0.026	0.049±0.017	0.097±0.058
O.B.QA	0.007±0.005	0.019±0.005	0.015±0.010	0.036±0.030
PiQA	0.005±0.003	0.008±0.002	0.013±0.004	0.025±0.011
WinO.	0.004±0.003	0.004±0.004	0.013±0.003	0.016±0.007
WSC	0.032±0.027	0.022±0.032	0.100±0.095	0.151±0.045
NLI	0.024±0.021	0.052±0.035	0.069±0.052	0.066±0.043
RTE	0.014±0.005	0.042±0.017	0.006±0.003	0.048±0.018
MRPC	0.057±0.022	0.091±0.002	0.068±0.018	0.064±0.040
CoLA	0.045±0.011	0.040±0.023	0.038±0.024	0.124±0.016
SST	0.031±0.023	0.079±0.097	0.062±0.066	0.039±0.025
CB	0.030±0.008	0.012±0.008	0.060±0.015	0.074±0.037
WiC	0.009±0.008	0.012±0.009	0.013±0.009	0.011±0.009
Avg	0.022±0.016	0.032±0.027	0.039±0.027	0.058±0.039

slightly larger differences (0.045 and 0.032, respectively), while all others show differences below 0.01. These results highlight the lightweight nature of the watermarking process based on model editing, which preserves the models’ original capabilities with only minimal performance variation.

Aligning Anchor Samples with Bit Vectors Maintains Sentence-Level and Lexical Understanding Utility. As the process involves aligning the hidden representations of anchor samples with corresponding bit vectors, we examine whether injecting SEAL watermarks affects the models’ sentence-level and lexical understanding capabilities. As shown in Table 4 (Line 9-15), aligning anchor embeddings with specific bit vectors has only a minimal impact on both sentence-level and lexical understanding tasks. When injecting 64-bit watermarks, the performance differences across all evaluated benchmarks remain within 0.06, with the largest deviation observed on the MRPC task (0.057). These results further confirm that the alignment process is effectively harmless to the models’ original understanding capabilities.

SEAL Maintains Model Utility Across Different Watermark Lengths. We further investigate whether increasing the number of injected watermark bits affects the models’ original performance. As shown in Table 4, although the average performance difference slightly increases with the watermark length, it causes negligible influence to the original models’ capabilities. Specifically, the average deviation rises modestly from 0.022 to 0.058 as the number of injected bits increases from 64 to 512. This behavior is expected, since embedding longer bit sequences requires aligning more anchor samples with bit vectors, which may introduce minimal noise into the model representations. Nevertheless, even at 512 bits, the observed degradation is marginal, further confirming that SEAL effectively preserves model utility across different watermark capacities.

6.4. RQ4: SEAL Efficiency

We further evaluate the **Efficiency** of SEAL in terms of both runtime and memory usage, and compare it against existing watermarking and fingerprinting methods. For fair comparison, we first measure efficiency by inserting and verifying a 1-bit watermark, as prior methods are limited to carrying a single bit of information. We then analyze runtime scalability with respect to the number of embedded bits.

TABLE 5: Runtime comparison of watermark inserting and verification. “All” reports the total runtime (in seconds).

Evaluation	Methods	Insertion	Verification	All
White-box	Gradient	-	28.25	28.25
	Huref	-	62.94	62.94
	Reef	-	13.94	13.94
	SEAL(W)	34.32	0.027	34.35
Black-box	Trap	-	3391.18	3391.18
	MET	-	48.01	48.01
	LLMMMap	-	39.72	39.72
	IF	20.72	18.80	39.52
	SEAL(B)	34.82	1.129	35.93

SEAL is Efficient to Embed and Verify in Runtime. As shown in Table 5, SEAL provides high runtime efficiency in both white-box and black-box settings. In the white-box case, SEAL completes insertion and verification in 34.35 seconds, which is comparable to Gradient and nearly 2× faster than Huref. Although Reef verifies faster (13.94 seconds), it does not perform watermark insertion. Once embedded, SEAL verifies in only 0.027 seconds, nearly 500× faster than Huref. In the black-box setting, SEAL also outperforms existing methods. It completes insertion and verification in 35.93 seconds, about 4 seconds faster than IF and LLMMMap and 13 seconds faster than MET, while Trap requires over 3000 seconds. Overall, SEAL offers a balanced, scalable, and low-latency runtime design across both access regimes.

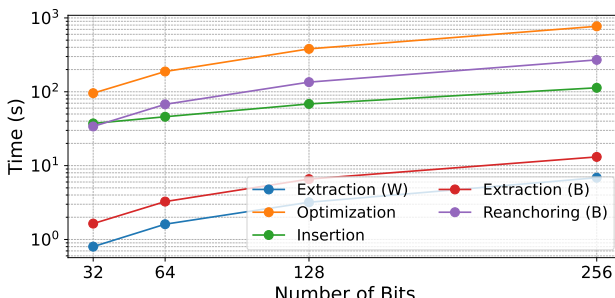


Figure 4: Efficiency study of watermark insertion and verification for different bit lengths in runtime.

We analyze SEAL’s runtime scalability with respect to the number of embedded bits. The pipeline is divided into four stages: (1) optimization of anchor-bit alignment, (2) insertion of parameter updates, (3) reanchoring of sentinel weights, and (4) extraction of watermark bits. Figure 4

reports the runtime of each stage under both white-box and black-box settings.

The insertion stage behaves similarly across settings, while extraction differs: black-box extraction operates on output logits, whereas white-box extraction directly reads latent representations. Reanchoring is required only in the black-box setting and adds modest overhead.

SEAL is Scalable to Embed Multiple Bits. Figure 4 shows how SEAL’s runtime scales with watermark size. The anchor-bit optimization stage dominates the cost, accounting for over half of the total runtime (e.g., 188.11 seconds for a 64-bit watermark, compared to 116.77 seconds for all other stages combined). This cost can be further reduced by performing optimization *offline* on batches of anchor candidates.

The insertion stage scales near-sublinearly with the number of bits, and extraction is inexpensive (6.86 seconds and 13.12 seconds for a 256-bit watermark in white-box and black-box settings). The reanchoring stage, required only for black-box verification, adds overhead but remains far cheaper than optimization. Overall, SEAL provides efficient and scalable multi-bit embedding and verification.

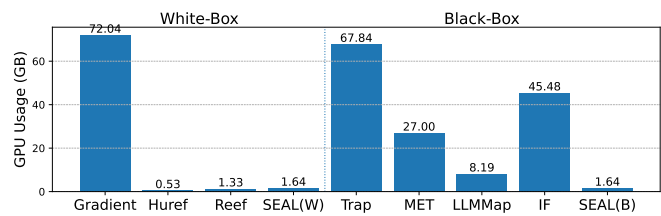


Figure 5: GPU memory usage (GB) during watermark insertion and verification.

SEAL Watermark is GPU-Efficient. As shown in Figure 5, SEAL requires only about 1.6 GB of GPU memory in both white- and black-box settings, which is comparable to Reef and Huref and far lower than Gradient (72 GB). In the black-box case, SEAL also remains at 1.6 GB, whereas methods such as Trap and IF consume up to 68 GB and 45 GB. These results show that SEAL offers fast embedding and verification with an extremely small GPU footprint, making it practical for real-world deployment.

6.5. RQ5: Hyperparameter Analysis

TABLE 6: Effectiveness of the reanchoring mechanism.

Models	Without Reanchoring			With Reanchoring		
	BER↓	BSE↑	BST↓	BER↓	BSE↑	BST↓
LLaMA2-7B	6.250	0.004	0.003	1.563	0.005	0.002
LLaMA3-8B	15.625	0.007	0.004	1.563	0.016	0.007
Qwen2.5-7B	7.813	0.004	0.002	0.000	0.006	0.001
Mistral-7B	4.688	0.008	0.005	1.563	0.010	0.004
Deepseek-7B	10.938	0.005	0.001	0.000	0.007	0.001

Effectiveness of Black-Box Reanchoring. Table 6 shows that reanchoring is crucial for accurate black-box extraction. Without it, BER ranges from 4.688% to 15.625% across

LLMs. After reanchoring the sentinel weights, BER drops to 1.563% (one error in 64 bits) or even 0.000%. Reanchoring also improves bit separability. For LLaMA3-8B, BSE increases from 0.007 to 0.016 (more than 2 \times). These results demonstrate that reanchoring restores the impact of bit vectors on output logits even after fine-tuning, enabling reliable black-box watermark recovery.

TABLE 7: Impact of anchor-sample selection.

Evaluation	Selection	Before SFT			After SFT		
		BER \downarrow	BSE \uparrow	BST \downarrow	BER \downarrow	BSE \uparrow	BST \downarrow
White-box	High-confidence	0.000	0.058	0.782	0.000	0.041	0.376
	Low-confidence	0.000	0.036	0.620	0.000	0.024	0.263
	Random	0.000	0.036	0.665	0.000	0.027	0.273
Black-box	High-confidence	0.000	0.012	0.002	1.563	0.005	0.002
	Low-confidence	0.000	0.009	0.002	15.625	0.003	0.002
	Random	0.000	0.010	0.002	6.250	0.003	0.002

Selecting High-Confidence Anchors Improves Watermark Robustness. To justify our choice of anchor samples for watermark embedding, we evaluate three strategies for selecting *(subject, relation, object)* triplets from the CounterFact dataset during SEAL injection. The *high-confidence* strategy selects samples whose objects already have the highest model-predicted probabilities; the *low-confidence* strategy selects those with the lowest probabilities. *Random* sampling serves as a reference.

As shown in Table 7, using high-confidence samples yields the most reliable extraction under SFT in both white- and black-box settings. In the black-box case, this strategy attains a post-SFT BER of 1.563%, whereas low-confidence and random samples lead to much higher BERs (15.625% and 6.250%). This supports using high-confidence samples as anchors, since low-confidence ones bias the optimization toward fitting target outputs rather than aligning latent embeddings with the bit vectors.

TABLE 8: Watermark extraction across insertion layers.

Evaluation	Insert Layers	Before SFT			After SFT		
		BER \downarrow	BSE \uparrow	BST \downarrow	BER \downarrow	BSE \uparrow	BST \downarrow
white-box	30	0.000	0.228	0.750	0.000	0.181	0.590
	15	0.000	0.035	0.651	0.000	0.061	0.605
	5	0.000	0.005	0.639	0.000	0.003	0.564
	28,29,30	0.000	0.008	0.772	1.563	0.003	0.484
	13,14,15	0.000	0.011	0.694	0.000	0.013	0.572
	3,4,5	0.000	0.007	0.206	0.000	0.007	0.193
black-box	5,15,30	0.000	0.038	0.782	0.000	0.021	0.633
	30	0.000	0.013	0.002	7.813	0.006	0.003
	15	14.063	0.005	0.003	32.813	0.004	0.003
	5	35.938	0.003	0.002	48.438	0.002	0.002
	28,29,30	0.000	0.011	0.003	4.688	0.004	0.003
	13,14,15	23.438	0.004	0.003	28.125	0.003	0.002
	3,4,5	40.625	0.001	0.001	45.313	0.002	0.001
	5,15,30	0.000	0.012	0.002	1.563	0.005	0.002

Selecting Proper Insertion Layers Enhances Watermark Robustness. We examine how different configurations of insertion layers affect watermark extraction. We compare single-layer and multi-layer strategies by embedding SEAL into transformer layers at various depths, and evaluate watermark extraction performance before and after SFT.

As shown in Table 8, all configurations achieve perfect white-box extraction (BER = 0) before SFT, with only minimal degradation afterward. In contrast, layer choice matters substantially in the black-box setting. Watermarks inserted into lower layers are far more fragile, yielding high BER even before SFT (e.g., 35.94% at layer (5) and 40.63% at (3,4,5)), whereas deeper layers such as (15) or (30) reduce BER to 14.06% and 0.00%. This is because black-box verification depends on the watermark’s influence on output logits, and lower-layer modifications have limited effect on the final output space.

We also find that distributing watermark updates across multiple layers improves robustness to SFT. For instance, spreading updates across (28,29,30) or (13,14,15) yields post-SFT BERs of 4.69% and 28.13%, compared to 7.81% and 14.06% with single-layer insertion. Combining layers at different depths provides the strongest resilience: inserting into (5,15,30) reduces post-SFT BER to 0.00%. This demonstrates that multi-layer, cross-depth embedding significantly enhances SEAL’s robustness under fine-tuning and black-box verification.

7. Robustness to Knowledgeable Attackers

We evaluate a strong, knowledgeable adversary who (i) knows the SEAL mechanism and the set of layers used for insertion and (ii) attempts to erase the watermark by fine-tuning only those layers.

TABLE 9: Impact of insertion layer selection.

Evaluation	Attack Layers	Before SFT			After SFT		
		BER \downarrow	BSE \uparrow	BST \downarrow	BER \downarrow	BSE \uparrow	BST \downarrow
white-box	26,27,28,29,30	0.000	0.158	0.775	0.000	0.133	0.625
	11,12,13,14,15	0.000	0.037	0.788	0.000	0.011	0.449
	10,9,8,7,6,5	0.000	0.010	0.787	0.000	0.002	0.250
black-box	5,15,30	0.000	0.187	0.763	0.000	0.156	0.636
	26,27,28,29,30	0.000	0.011	0.002	0.000	0.006	0.002
	11,12,13,14,15	0.000	0.011	0.002	3.125	0.004	0.002
	10,9,8,7,6,5	0.000	0.011	0.002	1.563	0.005	0.002
	5,15,30	0.000	0.012	0.002	0.000	0.006	0.002

Knowledgeable fine-tuning on known insertion layers does not remove SEAL. Table 9 shows that BER remains zero in all white-box cases, indicating that targeted updates cannot eliminate the multi-bit signal when hidden states are available for verification. In the black-box setting, BER increases only slightly for a few layer groups (e.g., up to 3.125), while high-level or cross-depth insertions (e.g., [30, 15, 5]) remain fully recoverable (BER = 0).

This robustness stems from two factors. First, SEAL distributes watermark information across semantic subspaces and multiple depths, making localized fine-tuning insufficient to remove the signal. Second, adversaries lack the defender’s secret anchor samples and optimization targets, so their fine-tuning cannot replicate the alignment required to erase the watermark without harming model utility. Thus, even knowing the insertion layers is insufficient: without access to the hidden anchors, no practical fine-tuning attack can reliably eliminate SEAL’s multi-bit watermark.

8. Conclusion

We presented SEAL, a subspace-anchored watermarking framework that embeds multi-bit signatures into the latent space of LLMs without altering their behavior. By aligning factual anchor representations with orthogonal bit vectors, SEAL achieves functionally harmless and persistent watermarking resilient to various model modifications. It supports both white-box verification via hidden-state inspection and black-box verification via Bayesian reanchoring, which reliably recovers watermarks under model drift. Experiments show that SEAL achieves near-perfect lineage identification (AUC = 1.00) and very low bit-error rates (< 1.21 %) while maintaining model utility, making it a practical solution for LLM ownership protection.

References

- [1] J. Achiam, S. Adler, S. Agarwal, L. Ahmad, I. Akkaya, F. L. Aleman, D. Almeida, J. Altenschmidt, S. Altman, S. Anadkat *et al.*, “Gpt-4 technical report,” *arXiv preprint arXiv:2303.08774*, 2023.
- [2] A. Research, “Model card addendum: Claude 3.5 haiku and upgraded claude 3.5 sonnet,” Anthropic, Tech. Rep., 2024, technical Report. [Online]. Available: <https://assets.anthropic.com/m/1cd9d098ac3e6467/original/Claude-3-Model-Card-October-Addendum.pdf>
- [3] H. Touvron, L. Martin, K. Stone, P. Albert, A. Almahairi, Y. Babaei, N. Bashlykov, S. Batra, P. Bhargava, S. Bhosale *et al.*, “Llama 2: Open foundation and fine-tuned chat models,” *arXiv preprint arXiv:2307.09288*, 2023.
- [4] A. Dubey, A. Jauhri, A. Pandey, A. Kadian, A. Al-Dahle, A. Letman, A. Mathur, A. Schelten, A. Yang, A. Fan *et al.*, “The llama 3 herd of models,” *arXiv e-prints*, pp. arXiv-2407, 2024.
- [5] L. Ouyang, J. Wu, X. Jiang, D. Almeida, C. L. Wainwright, P. Mishkin, C. Zhang, S. Agarwal, K. Slama, A. Ray, J. Schulman, J. Hilton, F. Kelton, L. Miller, M. Simens, A. Askell, P. Welinder, P. Christiano, J. Leike, and R. Lowe, “Training language models to follow instructions with human feedback,” in *Proceedings of the 36th International Conference on Neural Information Processing Systems*, ser. NIPS ’22. Red Hook, NY, USA: Curran Associates Inc., 2022.
- [6] P. F. Christiano, J. Leike, T. B. Brown, M. Martic, S. Legg, and D. Amodei, “Deep reinforcement learning from human preferences,” in *Proceedings of the 31st International Conference on Neural Information Processing Systems*, ser. NIPS’17. Red Hook, NY, USA: Curran Associates Inc., 2017, p. 4302–4310.
- [7] J. Kirchenbauer, J. Geiping, Y. Wen, J. Katz, I. Miers, and T. Goldstein, “A watermark for large language models,” in *International Conference on Machine Learning*. PMLR, 2023, pp. 17 061–17 084.
- [8] S. Dathathri, A. See, S. Ghaisas, P.-S. Huang, R. McAdam, J. Welbl, V. Bachani, A. Kaskasoli, R. Stanforth, T. Matejovicova *et al.*, “Scalable watermarking for identifying large language model outputs,” *Nature*, vol. 634, no. 8035, pp. 818–823, 2024.
- [9] R. Zhang, S. S. Hussain, P. Neekhara, and F. Koushanfar, “{REMARK-LLM}: A robust and efficient watermarking framework for generative large language models,” in *33rd USENIX Security Symposium (USENIX Security 24)*, 2024, pp. 1813–1830.
- [10] S. Shao, Y. Li, Y. He, H. Yao, W. Yang, D. Tao, and Z. Qin, “Sok: Large language model copyright auditing via fingerprinting,” *arXiv preprint arXiv:2508.19843*, 2025.
- [11] I. Gao, P. Liang, and C. Guestrin, “Model equality testing: Which model is this api serving?” in *International Conference on Learning Representations*, 2025.
- [12] M. Gubri, D. Ulmer, H. Lee, S. Yun, and S. J. Oh, “TRAP: Targeted random adversarial prompt honeypot for black-box identification,” in *Findings of the Association for Computational Linguistics: ACL 2024*, L.-W. Ku, A. Martins, and V. Srikanth, Eds. Bangkok, Thailand: Association for Computational Linguistics, Aug. 2024, pp. 11 496–11 517. [Online]. Available: <https://aclanthology.org/2024.findings-acl.683/>
- [13] D. Pasquini, E. M. Kornaropoulos, and G. Ateniese, “Llmmmap: fingerprinting for large language models,” in *Proceedings of the 34th USENIX Conference on Security Symposium*, ser. SEC ’25. USA: USENIX Association, 2025.
- [14] B. Darvish Rouhani, H. Chen, and F. Koushanfar, “Deepsigns: An end-to-end watermarking framework for ownership protection of deep neural networks,” in *Proceedings of the twenty-fourth international conference on architectural support for programming languages and operating systems*, 2019, pp. 485–497.
- [15] T. Wang and F. Kerschbaum, “Riga: Covert and robust white-box watermarking of deep neural networks,” in *Proceedings of the web conference 2021*, 2021, pp. 993–1004.
- [16] Q. Guo, X. Zhu, Y. Ma, H. Jin, Y. Wang, W. Zhang, and X. Guo, “Invariant-based robust weights watermark for large language models,” 2025. [Online]. Available: <https://arxiv.org/abs/2507.08288>
- [17] Y. Adi, C. Baum, M. Cisse, B. Pinkas, and J. Keshet, “Turning your weakness into a strength: Watermarking deep neural networks by backdooring,” in *27th USENIX security symposium (USENIX Security 18)*, 2018, pp. 1615–1631.
- [18] M. Russinovich and A. Salem, “Hey, that’s my model! introducing chain & hash, an llm fingerprinting technique,” *arXiv preprint arXiv:2407.10887*, 2024.
- [19] J. Xu, F. Wang, M. Ma, P. W. Koh, C. Xiao, and M. Chen, “Instructional fingerprinting of large language models,” in *Proceedings of the 2024 Conference of the North American Chapter of the Association for Computational Linguistics: Human Language Technologies (Volume 1: Long Papers)*, K. Duh, H. Gomez, and S. Bethard, Eds. Mexico City, Mexico: Association for Computational Linguistics, Jun. 2024, pp. 3277–3306. [Online]. Available: <https://aclanthology.org/2024.nacl-long.180/>
- [20] Z. Zhang, L. Lyu, X. Ma, C. Wang, and X. Sun, “Fine-mixing: Mitigating backdoors in fine-tuned language models,” in *Findings of the Association for Computational Linguistics: EMNLP 2022*, Y. Goldberg, Z. Kozareva, and Y. Zhang, Eds. Abu Dhabi, United Arab Emirates: Association for Computational Linguistics, Dec. 2022, pp. 355–372. [Online]. Available: <https://aclanthology.org/2022.findings-emnlp.26/>
- [21] P. Lv, H. Ma, K. Chen, J. Zhou, S. Zhang, R. Liang, S. Zhu, P. Li, and Y. Zhang, “Mea-defender: a robust watermark against model extraction attack,” in *2024 IEEE Symposium on Security and Privacy (SP)*. IEEE, 2024, pp. 2515–2533.
- [22] K. Meng, D. Bau, A. Andonian, and Y. Belinkov, “Locating and editing factual associations in GPT,” *Advances in Neural Information Processing Systems*, vol. 36, 2022, arXiv:2202.05262.
- [23] E. Mitchell, C. Lin, A. Bosselut, C. Finn, and C. D. Manning, “Fast model editing at scale,” in *International Conference on Learning Representations*, 2022. [Online]. Available: <https://openreview.net/forum?id=0DcZxeWfOPT>
- [24] E. J. Hu, Y. Shen, P. Wallis, Z. Allen-Zhu, Y. Li, S. Wang, L. Wang, W. Chen *et al.*, “Lora: Low-rank adaptation of large language models,” *ICLR*, vol. 1, no. 2, p. 3, 2022.
- [25] S. Wang, L. Yu, and J. Li, “Lora-ga: Low-rank adaptation with gradient approximation,” *Advances in Neural Information Processing Systems*, vol. 37, pp. 54 905–54 931, 2024.
- [26] Y. Gu, L. Dong, F. Wei, and M. Huang, “Minillm: Knowledge distillation of large language models,” 2024. [Online]. Available: <https://arxiv.org/abs/2306.08543>

[27] H. Peng, X. Lv, Y. Bai, Z. Yao, J. Zhang, L. Hou, and J. Li, “Pre-training distillation for large language models: A design space exploration,” in *Proceedings of the 63rd Annual Meeting of the Association for Computational Linguistics (Volume 1: Long Papers)*, W. Che, J. Nabende, E. Shutova, and M. T. Pilehvar, Eds. Vienna, Austria: Association for Computational Linguistics, Jul. 2025, pp. 3603–3618. [Online]. Available: <https://aclanthology.org/2025.acl-long.181/>

[28] R. Zhang, J. Shen, T. Liu, H. Wang, Z. Qin, F. Han, J. Liu, S. Baumgartner, M. Bendersky, and C. Zhang, “PLaD: Preference-based large language model distillation with pseudo-preference pairs,” in *Findings of the Association for Computational Linguistics: ACL 2024*, L.-W. Ku, A. Martins, and V. Srikumar, Eds. Bangkok, Thailand: Association for Computational Linguistics, Aug. 2024, pp. 15 623–15 636. [Online]. Available: <https://aclanthology.org/2024.findings-acl.923/>

[29] G. Xiao, J. Lin, M. Seznec, H. Wu, J. Demouth, and S. Han, “Smoothquant: Accurate and efficient post-training quantization for large language models,” in *International conference on machine learning*. PMLR, 2023, pp. 38 087–38 099.

[30] R. Banner, Y. Nahshan, and D. Soudry, “Post training 4-bit quantization of convolutional networks for rapid-deployment,” *Advances in neural information processing systems*, vol. 32, 2019.

[31] J. Lin, J. Tang, H. Tang, S. Yang, W.-M. Chen, W.-C. Wang, G. Xiao, X. Dang, C. Gan, and S. Han, “Awq: Activation-aware weight quantization for on-device llm compression and acceleration,” *Proceedings of machine learning and systems*, vol. 6, pp. 87–100, 2024.

[32] E. Yang, L. Shen, G. Guo, X. Wang, X. Cao, J. Zhang, and D. Tao, “Model merging in llms, mllms, and beyond: Methods, theories, applications and opportunities,” *arXiv preprint arXiv:2408.07666*, 2024.

[33] Y. Li, Y. Ma, S. Yan, C. Zhang, J. Liu, J. Lu, Z. Xu, M. Chen, M. Wang, S. Zhan, J. Ma, X. Lai, Y. Luo, X. Bin, H. Ren, M. Han, W. Hao, B. Yi, L. Liu, B. Ma, X. Jia, zhou Xun, liang xiang, and Y. Wu, “Model merging in pre-training of large language models,” in *The Thirty-ninth Annual Conference on Neural Information Processing Systems*, 2025. [Online]. Available: <https://openreview.net/forum?id=HW55AwGEC8>

[34] A. H. Nobari, K. Alim, A. ArjomandBigdeli, A. Srivastava, F. Ahmed, and N. Azizan, “Activation-informed merging of large language models,” in *The Thirty-ninth Annual Conference on Neural Information Processing Systems*, 2025. [Online]. Available: <https://openreview.net/forum?id=T4qJuQCFAK>

[35] K. Meng, A. Sen Sharma, A. Andonian, Y. Belinkov, and D. Bau, “Mass editing memory in a transformer,” *The Eleventh International Conference on Learning Representations (ICLR)*, 2023.

[36] Y. Dai, Z. Ji, Z. Li, and S. Wang, “Eamet: Robust massive model editing via embedding alignment optimization,” 2025. [Online]. Available: <https://arxiv.org/abs/2505.11876>

[37] M. Geva, R. Schuster, J. Berant, and O. Levy, “Transformer feed-forward layers are key-value memories,” in *Proceedings of the 2021 Conference on Empirical Methods in Natural Language Processing*, 2021, pp. 5484–5495.

[38] B. Zeng, L. Wang, Y. Hu, Y. Xu, C. Zhou, X. Wang, Y. Yu, and Z. Lin, “Huref: Human-readable fingerprint for large language models,” *Advances in Neural Information Processing Systems*, vol. 37, pp. 126 332–126 362, 2024.

[39] R. Kuditipudi, J. Thickstun, T. Hashimoto, and P. Liang, “Robust distortion-free watermarks for language models,” *arXiv preprint arXiv:2307.15593*, 2023.

[40] V. S. Sadasivan, A. Kumar, S. Balasubramanian, W. Wang, and S. Feizi, “Can ai-generated text be reliably detected?” *arXiv preprint arXiv:2303.11156*, 2023.

[41] A. Pegoraro, C. Segna, K. Kumari, and A.-R. Sadeghi, “{DeepEclipse}: How to break {White-Box}{DNN-Watermarking} schemes,” in *33rd USENIX Security Symposium (USENIX Security 24)*, 2024, pp. 5287–5304.

[42] H. Yao, J. Lou, Z. Qin, and K. Ren, “Promptcare: Prompt copyright protection by watermark injection and verification,” in *2024 IEEE Symposium on Security and Privacy (SP)*. IEEE, 2024, pp. 845–861.

[43] Y. Yan, X. Pan, M. Zhang, and M. Yang, “Rethinking {White-Box} watermarks on deep learning models under neural structural obfuscation,” in *32nd USENIX Security Symposium (USENIX Security 23)*, 2023, pp. 2347–2364.

[44] J. Hills and S. Anadkat, “Using `logprobs` — openai cookbook,” https://cookbook.openai.com/examples/using_logprobs, 2023, accessed: 2025-11-10.

[45] Z. Li, D. Wu, S. Wang, and Z. Su, “Differentiation-based extraction of proprietary data from fine-tuned llms,” 2025. [Online]. Available: <https://arxiv.org/abs/2506.17353>

[46] R. W. Hamming, “Error detecting and error correcting codes,” *The Bell system technical journal*, vol. 29, no. 2, pp. 147–160, 1950.

[47] R. C. Bose and D. K. Ray-Chaudhuri, “On a class of error correcting binary group codes,” *Information and control*, vol. 3, no. 1, pp. 68–79, 1960.

[48] S. B. Wicker and V. K. Bhargava, *Reed-Solomon codes and their applications*. John Wiley & Sons, 1999.

[49] Q. Team, “Qwen2.5 technical report,” 2025. [Online]. Available: <https://arxiv.org/abs/2412.15115>

[50] M. Team, “Mistral 7b,” 2023. [Online]. Available: <https://arxiv.org/abs/2310.06825>

[51] D. Team, “Deepseek-v3 technical report,” *arXiv preprint arXiv:2412.19437*, 2024.

[52] R. Taori, I. Gulrajani, T. Zhang, Y. Dubois, X. Li, C. Guestrin, P. Liang, and T. B. Hashimoto, “Stanford alpaca: An instruction-following llama model,” 2023.

[53] N. Ding, Y. Chen, B. Xu, Y. Qin, S. Hu, Z. Liu, M. Sun, and B. Zhou, “Enhancing chat language models by scaling high-quality instructional conversations,” in *Proceedings of the 2023 Conference on Empirical Methods in Natural Language Processing*, H. Bouamor, J. Pino, and K. Bali, Eds. Singapore: Association for Computational Linguistics, Dec. 2023, pp. 3029–3051. [Online]. Available: <https://aclanthology.org/2023.emnlp-main.183/>

[54] Y. Jiang, C. Chan, M. Chen, and W. Wang, “Lion: Adversarial distillation of proprietary large language models,” in *Proceedings of the 2023 Conference on Empirical Methods in Natural Language Processing*, H. Bouamor, J. Pino, and K. Bali, Eds. Singapore: Association for Computational Linguistics, Dec. 2023, pp. 3134–3154. [Online]. Available: <https://aclanthology.org/2023.emnlp-main.189/>

[55] S. Zhang, X. Zhang, Z. Sun, Y. Chen, and J. Xu, “Dual-space knowledge distillation for large language models,” in *Proceedings of the 2024 Conference on Empirical Methods in Natural Language Processing*, Y. Al-Onaizan, M. Bansal, and Y.-N. Chen, Eds. Miami, Florida, USA: Association for Computational Linguistics, Nov. 2024, pp. 18 164–18 181. [Online]. Available: <https://aclanthology.org/2024.emnlp-main.1010/>

[56] J. Li, S. Nag, H. Liu, X. Tang, S. M. Sarwar, L. Cui, H. Gu, S. Wang, Q. He, and J. Tang, “Learning with less: Knowledge distillation from large language models via unlabeled data,” in *Findings of the Association for Computational Linguistics: NAACL 2025*, L. Chiruzzo, A. Ritter, and L. Wang, Eds. Albuquerque, New Mexico: Association for Computational Linguistics, Apr. 2025, pp. 2627–2641. [Online]. Available: <https://aclanthology.org/2025.findings-naacl.142/>

[57] B. Jacob, S. Kligys, B. Chen, M. Zhu, M. Tang, A. Howard, H. Adam, and D. Kalenichenko, “Quantization and training of neural networks for efficient integer-arithmetic-only inference,” in *Proceedings of the IEEE conference on computer vision and pattern recognition*, 2018, pp. 2704–2713.

- [58] Z. Wu, Y. Zhao, and H. Wang, “Gradient-based model fingerprinting for llm similarity detection and family classification,” *arXiv preprint arXiv:2506.01631*, 2025.
- [59] J. Zhang, D. Liu, C. Qian, L. Zhang, Y. Liu, Y. Qiao, and J. Shao, “Reef: Representation encoding fingerprints for large language models,” 2024. [Online]. Available: <https://arxiv.org/abs/2410.14273>
- [60] D. hyeon Yoon, M. Chun, T. Allen, H. Müller, M. Wang, and R. Sharma, “Intrinsic fingerprint of llms: Continue training is not all you need to steal a model!” 2025. [Online]. Available: <https://arxiv.org/abs/2507.03014>
- [61] A. Nasery, J. Hayase, C. Brooks, P. Sheng, H. Tyagi, P. Viswanath, and S. Oh, “Scalable fingerprinting of large language models,” in *The 1st Workshop on GenAI Watermarking*, 2025. [Online]. Available: <https://openreview.net/forum?id=ImrmzMDq5z>
- [62] K. Meng, D. Bau, A. Andonian, and Y. Belinkov, “Locating and editing factual associations in gpt,” in *Proceedings of the 36th International Conference on Neural Information Processing Systems*, ser. NIPS ’22. Red Hook, NY, USA: Curran Associates Inc., 2022.
- [63] D. Hendrycks, C. Burns, S. Basart, A. Zou, M. Mazeika, D. Song, and J. Steinhardt, “Measuring massive multitask language understanding,” 2021. [Online]. Available: <https://arxiv.org/abs/2009.03300>
- [64] C. Clark, K. Lee, M.-W. Chang, T. Kwiatkowski, M. Collins, and K. Toutanova, “Boolq: Exploring the surprising difficulty of natural yes/no questions,” *arXiv preprint arXiv:1905.10044*, 2019.
- [65] K. Sakaguchi, R. L. Bras, C. Bhagavatula, and Y. Choi, “Winogrande: An adversarial winograd schema challenge at scale,” *Communications of the ACM*, vol. 64, no. 9, pp. 99–106, 2021.
- [66] M. Roemmele, C. A. Bejan, and A. S. Gordon, “Choice of plausible alternatives: An evaluation of commonsense causal reasoning.” in *AAAI spring symposium: logical formalizations of commonsense reasoning*, 2011, pp. 90–95.
- [67] Y. Bisk, R. Zellers, J. Gao, Y. Choi *et al.*, “Piqa: Reasoning about physical commonsense in natural language,” in *Proceedings of the AAAI conference on artificial intelligence*, vol. 34, no. 05, 2020, pp. 7432–7439.
- [68] T. Mihaylov, P. Clark, T. Khot, and A. Sabharwal, “Can a suit of armor conduct electricity? a new dataset for open book question answering,” *arXiv preprint arXiv:1809.02789*, 2018.
- [69] P. Clark, I. Cowhey, O. Etzioni, T. Khot, A. Sabharwal, C. Schoenick, and O. Tafjord, “Think you have solved question answering? try arc, the ai2 reasoning challenge,” *arXiv preprint arXiv:1803.05457*, 2018.
- [70] A. Wang, A. Singh, J. Michael, F. Hill, O. Levy, and S. R. Bowman, “Glue: A multi-task benchmark and analysis platform for natural language understanding,” *arXiv preprint arXiv:1804.07461*, 2018.
- [71] A. Warstadt, A. Singh, and S. R. Bowman, “Neural network acceptability judgments,” *Transactions of the Association for Computational Linguistics*, vol. 7, pp. 625–641, 2019. [Online]. Available: <https://aclanthology.org/Q19-1040/>
- [72] W. B. Dolan and C. Brockett, “Automatically constructing a corpus of sentential paraphrases,” in *Proceedings of the Third International Workshop on Paraphrasing (IWP2005)*, 2005. [Online]. Available: <https://aclanthology.org/I05-5002/>
- [73] M.-C. De Marneffe, M. Simons, and J. Tonhauser, “The commitmentbank: Investigating projection in naturally occurring discourse,” in *proceedings of Sinn und Bedeutung*, vol. 23, no. 2, 2019, pp. 107–124.
- [74] M. T. Pilehvar and J. Camacho-Collados, “Wic: the word-in-context dataset for evaluating context-sensitive meaning representations,” *arXiv preprint arXiv:1808.09121*, 2018.

Appendix A.

Comparison Pool

We list the comparison pool used for model lineage identification in Table 10.

Appendix B.

Derivation of Bayesian Reanchoring

We derive the closed-form posterior mean used in our Bayesian reanchoring procedure in Equation (23), under standard Gaussian assumptions.

Problem Setup. Let $w \in \mathbb{R}^m$ denote the unknown sentinel projection vector under the current (potentially fine-tuned) model. We assume access to:

- A prior estimate w_{sig} computed during the white-box stage.
- A sample mean drift μ_{Δ} estimated from paired logit differences $\Delta\mathcal{L}_k = L_k^D - L_k^W$ across K reference prompts.

Our goal is to infer the most likely value of w given the observed drift μ_{Δ} .

Bayesian Formulation. We place the following Gaussian prior on w :

$$p(w) = \mathcal{N}(w_{\text{sig}}, \lambda^{-1} I), \quad (27)$$

and model the likelihood of the observed logit shift as:

$$p(\mu_{\Delta} | w) = \mathcal{N}(w - w_{\text{sig}}, \rho \Sigma_{\Delta}), \quad (28)$$

which reflects the assumption that the empirical drift μ_{Δ} is a noisy observation of the true shift $w - w_{\text{sig}}$.

Applying Bayes’ rule, the posterior is proportional to:

$$p(w | \mu_{\Delta}) \propto p(\mu_{\Delta} | w) \cdot p(w). \quad (29)$$

Taking the negative log-posterior (up to constants), we obtain the following objective:

$$\begin{aligned} \mathcal{L}(w) = & \frac{1}{2\rho} (\mu_{\Delta} - (w - w_{\text{sig}}))^{\top} \Sigma_{\Delta}^{-1} (\mu_{\Delta} - (w - w_{\text{sig}})) \\ & + \frac{\lambda}{2} \|w - w_{\text{sig}}\|_2^2. \end{aligned} \quad (30)$$

Closed-Form Solution (MAP). Expanding the quadratic terms and minimizing $\mathcal{L}(w)$ yields the maximum a posteriori (MAP) estimate:

$$(\rho \Sigma_{\Delta} + \lambda I)w = \rho \Sigma_{\Delta}(\mu_{\Delta} + w_{\text{sig}}) + \lambda w_{\text{sig}}. \quad (31)$$

Solving for w gives:

$$w = (\rho \Sigma_{\Delta} + \lambda I)^{-1} [\rho \Sigma_{\Delta}(\mu_{\Delta} + w_{\text{sig}}) + \lambda w_{\text{sig}}]. \quad (32)$$

To remove uniform offsets (which do not affect verification), we apply a zero-mean projection:

$$P = I - \frac{\mathbf{1}\mathbf{1}^{\top}}{m}, \quad (33)$$

and express the final reanchored vector as:

$$w^* = (\rho \Sigma_{\Delta} + \lambda I)^{-1} (w_{\text{sig}} + P\mu_{\Delta} + \lambda Pw_{\text{sig}}), \quad (34)$$

which is the form used in Equation (23).

TABLE 10: Comparison pool used for model lineage identification. Each column represents a target model, and each row lists the candidate models evaluated for determining whether they are derivatives of the corresponding target model.

LLaMA2-7B	Qwen2.5-7B	LLaMA3-8B	Mistral-7B	Deepseek-7B	Qwen2.5-14B
LLaMA2-7B (PEFT) - alpaca	Qwen2.5-7B (PEFT) - alpaca	LLaMA3-8B (PEFT) - alpaca	Mistral-7B (PEFT) - alpaca	Deepseek-7B (PEFT) - alpaca	qwen-14b (PEFT) - alpaca
LLaMA2-7B (PEFT) - shareGPT	Qwen2.5-7B (PEFT) - shareGPT	LLaMA3-8B (PEFT) - shareGPT	Mistral-7B (PEFT) - shareGPT	Deepseek-7B (PEFT) - shareGPT	qwen-14b (PEFT) - shareGPT
LLaMA2-7B (SFT) - alpaca	Qwen2.5-7B (SFT) - alpaca	LLaMA3-8B (SFT) - alpaca	Mistral-7B (SFT) - alpaca	Deepseek-7B (SFT) - alpaca	qwen-14b (SFT) - alpaca
LLaMA2-7B (SFT) - shareGPT	Qwen2.5-7B (SFT) - shareGPT	LLaMA3-8B (SFT) - shareGPT	Mistral-7B (SFT) - shareGPT	Deepseek-7B (SFT) - shareGPT	qwen-14b (SFT) - shareGPT
LLaMA2-7B (DT) - LLaMA	Qwen2.5-7B (DT) - alpaca	LLaMA3-8B (DT) - alpaca	Mistral-7B (DT) - alpaca	Deepseek-7B (DT) - alpaca	qwen-14b (DT) - alpaca
LLaMA2-7B (DT) - shareGPT	Qwen2.5-7B (DT) - shareGPT	LLaMA3-8B (DT) - shareGPT	Mistral-7B (DT) - shareGPT	Deepseek-7B (DT) - shareGPT	qwen-14b (DT) - shareGPT
Qwen2.5-7B	LLaMA2-7B	Qwen2.5-7B	Qwen2.5-7B	Qwen2.5-7B	Qwen2.5-7B
LLaMA3-8B	LLaMA3-8B	LLaMA2-7B	LLaMA3-8B	LLaMA3-8B	LLaMA3-8B
LLaMA2-13B	LLaMA2-13B	LLaMA2-13B	LLaMA2-13B	LLaMA2-13B	LLaMA2-13B
Mistral-7B	Mistral-7B	Mistral-7B	Mistral-7B	Mistral-7B	Mistral-7B
Deepseek-7B	Deepseek-7B	Deepseek-7B	Deepseek-7B	Deepseek-7B	Deepseek-7B
Gemma-7B	Gemma-7B	Gemma-7B	Gemma-7B	Gemma-7B	Gemma-7B

Appendix C. Error Correction Coding (ECC) for Enhanced Reliability

Although SEAL already achieves high watermark extraction accuracy under both white-box and black-box settings, further reliability can be achieved by integrating ECC into the bit-level representation. Specifically, each k -bit watermark segment can be encoded into an n -bit ECC codeword (e.g., using Hamming [46] or BCH codes [47]), which allows the verifier to correct a small number of bit flips during extraction. We anticipate that, this design is particularly beneficial under noisy or partially compromised conditions, where quantization, model merging, or low-bit retrieval may induce minor bit errors.

Notice that integrating ECC does not change SEAL’s embedding procedure or security assumptions. The encoder simply maps the original watermark bits into a redundant but error-tolerant format before optimization, and the verifier applies standard ECC decoding upon recovery. In practice, a lightweight (n, k) configuration such as $(128, 64)$ provides strong correction capability with less than $2\times$ bit overhead, while maintaining the same optimization cost and watermark invisibility. This enhancement ensures that SEAL remains verifiable even when a small portion of the embedded bits are perturbed, further improving robustness against extreme post-deployment model transformations.

Appendix D. Details of Evaluation Metrics for Lineage Identification

We introduce the details of the evaluation metrics used in evaluating the effectiveness of model lineage identification.

- **Area Under the ROC Curve (AUC).** This metric quantifies the overall capability of distinguishing between *derivative* and *independent* models. A higher AUC indicates stronger discriminative power.
- **Partial AUC (pAUC).** This metric measures the performance under a low false positive rate (FPR) regime, typically in the range $[0, 0.05]$, focusing on the method’s robustness against false positives.
- **Mahalanobis Distance (MD).** This metric computes the mean distance between the derived score distributions of

derivative and independent models. A higher MD reflects better separation between model lineages.